Atomic Layer Deposition of Oxide Films
– Growth, Characterisation and Reaction Mechanism Studies

Raija Matero

Laboratory of Inorganic Chemistry
Department of Chemistry
Faculty of Science
University of Helsinki
Finland

Academic Dissertation
To be presented for public criticism, with the permission of the Faculty of Science of the University of Helsinki, in Auditorium A129 of the Department of Chemistry, A. I. Virtasen aukio 1, on December 17th, 2004 at 12 o'clock noon.

Helsinki 2004

ISBN 952-91-8113-2 (paperback)
ISBN 952-10-2239-6 (pdf)
http://ethesis.helsinki.fi
Helsinki 2004
Yliopistopaino

Abstract

Atomic layer deposition was used to grow Al_2O_3, TiO_2 and ZrO_2 thin films. The mechanism of film growth was studied with a quadrupole mass spectrometer (QMS) and a quartz crystal microbalance (QCM). A brief literature review on the ALD growth of binary oxides and on *in situ* studies on selected oxide processes is presented as background.

The effect of water dose on the growth of Al_2O_3, TiO_2, ZrO_2 and Ta_2O_5 was studied. The increased water dose increased the growth rate in all cases. According to the analysis data, it did not seem to affect the film properties.

Al_2O_3 and TiO_2 films were deposited for corrosion protection studies. Although ALD grown Al_2O_3 is amorphous and there should not be any pinholes, it did not work as a protective coating against corrosive media. TiO_2 films are crystalline, and the corrosive media was able to penetrate through the coating and cause corrosion of the underlying substrate. The good characteristics of both materials were combined as Al_2O_3 – TiO_2 multilayer structures, which resisted corrosion better than the single oxides.

The reaction mechanism studies on Me_2AlCl–D_2O and $TiCl_4$–D_2O ALD processes were carried out using a combination of QMS and QCM integrated to the ALD reactor. QMS gives information about the gaseous products formed in the surface reactions involved in the film growth. QCM, in turn, monitors changes in the film mass.

ZrO_2 films were deposited using water and new alkoxide precursors: $Zr(dmae)_4$, $Zr(dmae)_2(O^tBu)_2$ and $Zr(dmae)_2(O^iPr)_2$. The reaction mechanism was studied using QMS–QCM. The precursors seem to decompose, so the growth can not be regarded as ideal ALD.

Preface

I wish to thank the two professors, Markku Leskelä and Mikko Ritala, for supervising and guiding me during the years that were needed to complete this thesis. I appreciate their patience with me.

I am grateful to all those in the Laboratory of Inorganic Chemistry who have helped me during this work. I owe warm thanks to Dr. Antti Rahtu for sharing with me his knowledge of reaction mechanism studies. I would like to thank Markku Talja for his help with organic chemistry, and Teemu Alaranta and Kjell Knapas for carrying out part of the QCM–QMS experiments. I also wish to acknowledge Dr. Janne Jokinen and Dr. Timo Sajavaara for TOF-ERDA and NRB measurements.

I would like to thank all my co-authors at the Helsinki University of Technology, University of Liverpool and Epichem Oxides and Nitrides.

The National Technology Agency of Finland (Tekes), and Jenny and Antti Wihuri foundation are acknowledged for financial support.

Special thanks go to Karl Fazer, I would not have made it without you.

Vantaa, November 2004

Raija Matero

List of Publications

I Matero, R., Rahtu, A., Ritala, M., Leskelä, M. and Sajavaara, T.
Effect of Water Dose on the Atomic Layer Deposition Rate of Oxide Thin Films
Thin Solid Films 368 (2000) 1.

II Matero, R., Ritala, M., Leskelä, M., Salo, T., Aromaa, J. and Forsén, O.
Atomic Layer Deposited Thin Films for Corrosion Protection
Journal de Physique IV 9 (1999) Pr8-493.

III Matero, R., Rahtu, A. and Ritala, M.
In situ Studies on the Atomic Layer Deposition of Al_2O_3 from Dimethylaluminium chloride and Water
Langmuir, submitted

IV Matero, R., Rahtu, A. and Ritala, M.
In situ Quadrupole Mass Spectrometry and Quartz Crystal Microbalance Studies on the Atomic Layer Deposition of Titanium Dioxide from Titanium Tetrachloride and Water
Chemistry of Materials 13 (2001) 4506.

V Matero, R., Ritala, M., Leskelä, M., Jones, A.C., Williams, P.A., Bickley, J.F., Steiner, A., Leedham, T.J. and Davies, H.O.
Atomic Layer Deposition of ZrO_2 Thin Films Using a New Alkoxide Precursor
Journal of Non-Crystalline Solids 303 (2002) 24.

VI Matero, R., Ritala, M., Leskelä, M., Sajavaara, T., Jones, A.C. and Roberts, J.L.
Evaluation of New Aminoalkoxide Precursors for Atomic Layer Deposition — Growth of ZrO_2 Thin Films and Reaction Mechanism Studies
Chemistry of Materials, in press

List of Abbreviations and Symbols

acac	acetylacetonate, 2,4-pentanedione
AES	Auger electron spectroscopy
ALD	Atomic layer deposition
ALE	Atomic layer epitaxy
Bu	butyl, $–CH_2CH_2CH_2CH_3$
Cp	cyclopentadienyl, C_5H_5
CVD	Chemical vapour deposition
dmae	dimethylaminoethoxide, $–OCH_2CH_2N(CH_3)_2$
EPMA	Electron-probe microanalysis
Et	ethyl, $–CH_2CH_3$
FReS	Forward recoil spectrometry
Glycol	CH_2OHCH_2OH
^{i}Pr	isopropyl, $–CH(CH_3)_2$
Me	methyl, $–CH_3$
mmp	1-methoxy-2-methyl-2-propanolate, $–OC(CH_3)_2CH_2OCH_3$
NRA	Nuclear resonance analysis
NRB	Nuclear resonance broadening
OEt	ethoxide, $–OCH_2CH_3$
O^{i}Pr	isopropoxide, $–OCH(CH_3)_2$
Pr	propyl, $–CH_2CH_2CH_3$
QCM	Quartz crystal microbalance
QMS	Quadrupole mass spectrometer
RBS	Rutherford backscattering spectroscopy
SIMS	Secondary ion mass spectrometry
tbaoac	tert-butylacetoacetate
^{t}Bu	tert-butyl, $–C(CH_3)_3$
thd	tetramethylheptanedione
TOF-ERDA	Time-of-flight elastic recoil detection analysis
XPS	X-ray photoelectron spectroscopy
XRD	X-ray diffraction
XRF	X-ray fluorescence

CONTENTS

1. Introduction

Atomic layer deposition (ALD), previously called atomic layer epitaxy (ALE), is a unique method for depositing high quality thin films[1–4]. The characteristic feature of ALD distinguishing it from the closely related CVD technique is the alternate supply of gaseous precursors on the substrate. In ALD, the reactants are pulsed onto the substrates one at a time. Between the reactant pulses, excess reactants and reaction by-products are purged out or evacuated. The experimental parameters, i.e. substrate temperature, reactant pressures and their exposure times, and the lengths of the purging periods, are adjusted in a way that all the surface reactions are saturative and purging steps are complete, removing all the other precursor molecules except those which have chemisorbed or undergone exchange reactions with the surface groups. Under these conditions, the film growth is self-limiting which ensures that uniform films with excellent conformality can be deposited even onto complex-shaped large-area substrates, and that film thicknesses can be controlled accurately simply by the number of reaction cycles repeated. The major limitation of ALD is its slowness; growth rates of only 100 – 300 nm/h are typically achieved. However, this problem is compensated to some extent by the excellent large-area/large-batch capability of ALD, which makes it possible to achieve competitive productivities.

ALD was originally invented for depositing polycrystalline and amorphous thin films for electroluminescent (EL) displays[5] and it is still used for their production. The use of ALD has been examined and demonstrated also in other applications which have been recently described in reviews focusing on different areas: nanotechnology[6], electronic and optoelectronic materials[7] and catalysts[8]. Recently, ALD has been widely studied for silicon-based microelectronics.[9] Dielectric metal oxides — or high-k oxides as they are called due to their high permittivity — have been in key role. Research groups all over the world have been searching for a material to replace SiO_2 in integrated circuits. Other applications in integrated circuits include DRAM capacitors, metal barriers and gate metals. It is also likely that ALD finds applications in other areas, such as magnetic recording heads, optics, protective coatings, and micro-electromechanical systems, but more research is still needed until those goals are achieved.

This thesis is focused on two areas: ALD film growth, and *in situ* reaction mechanism studies using a quartz crystal microbalance (QCM) and a quadrupole mass spectrometer (QMS). It concentrates on three materials: Al_2O_3[I-III] TiO_2[I,II,IV] and ZrO_2[I,V,VI], but other oxides[I] are also discussed briefly. The effect of increased water dose on the growth rate of Al_2O_3 and several other oxides is discussed.[I] Al_2O_3 and TiO_2 were studied as protective coatings against corrosion.[II] New aminoalkoxide Zr precursors were tested for the growth of ZrO_2.[V,VI] The *in situ* studies comprise the Al_2O_3[III], TiO_2[IV] and ZrO_2[VI] processes.

2. ALD of Binary Dielectric Oxide Films

This chapter presents a short retrospective review on ALD of binary dielectric oxides. The dielectric oxide films deposited by ALD are summarised in Table 1. The growth process and characteristics of the film materials relevant to this study, namely Al_2O_3, TiO_2 and ZrO_2, are presented in more detail in Tables 2, 3 and 4.

Table 1. Binary dielectric oxide materials deposited by ALD

Film Material	Metal Source	Oxygen Source
Al_2O_3	$AlCl_3$[10-16] Me_3Al[16-27] Me_2AlCl[28] $Al(OEt)_3$[13] $Al(OPr)_3$[13] $Me_2Al(O^iPr)$[29]	H_2O[12-14,17-20,28-29] H_2O_2[21-25] O_2[10-11,13] O_3[26] MeOH[13] ^{t}BuOH[13,15] BuOH[13] Glycol[13] N_2O[25] ^{i}PrOH[27] $Al(OEt)_3$[16] $Al(O^iPr)_3$[16]
TiO_2	$TiCl_4$[30-33] TiI_4[34-37] $Ti(OMe)_4$[38] $Ti(OEt)_4$[41] $Ti(O^iPr)_4$[39-40]	H_2O[30-31,38-41] H_2O_2[32-35] O_2[36-37]
ZrO_2	$ZrCl_4$[42-43] ZrI_4[44] $Zr(O^tBu)_4$[45-46] $Zr(dmae)_4$[VI] $Zr(dmae)_2(O^tBu)_2$[V,VI] $Zr(dmae)_2(O^iPr)_2$[VI] $Zr(acac)_4$[49] $Zr(thd)_4$[47] $Zr(tbaoac)_4$[49] $CpZrMe_2$[47-48] $CpZrCl_2$[47] $Zr(NMe_2)_4$[50] $Zr(NEt_2)_4$[50] $Zr(NMeEt)_4$[50] $ZrCl_2[N(SiMe_3)_2]_2$[51]	H_2O[42-45,48,50-51,V,VI] H_2O_2[43-44] O_2[46,49] O_3[47]
HfO_2	$HfCl_4$[52] HfI_4[58-60] $Hf(O^tBu)_4$[61-62] $Hf(mmp)_4$[53] $Hf(O^tBu)_2(mmp)_2$[54] $Hf(ONEt_2)_4$[57] $Hf(NMe_2)_4$[50] $Hf(NEt_2)_4$[50] $Hf(NMeEt)_4$[50,56] $Hf(NO_3)_4$[55]	H_2O[50,52-58] H_2O_2[58] O_2[59-61] O_3[62]

Table 1. continued Binary dielectric oxide materials deposited by ALD

Film Material	Metal Source	Oxygen Source
Ta_2O_5	$TaCl_5$[63-67] TaI_5[68-69] $Ta(OEt)_5$[70] $Ta(NMe_2)_5$[71] $Ta(NEt)(NEt_2)_3$[71]	H_2O[63-66,68, 70-71] H_2O_2[68] O_2[69] $Ta(OEt)_5$[67]
Nb_2O_5	$Nb(OEt)_5$[96]	H_2O[96]
SiO_2	$SiCl_4$[72-77] Si_2Cl_6[78] $Si(NCO)_4$[79-80] $CH_3OSi(NCO)_3$[81]	H_2O[72-74,79] H_2O_2[80-81] H_2O(pyridine catalysed)[75-76,78] H_2O(NH_3 catalysed)[77]
Sc_2O_3	$Sc(thd)_3$[91]	O_3[91]
Y_2O_3	$Y(thd)_3$[85-86] $Y(thd)_3$(bipyridyl)[86] $Y(thd)_3$(1,10-phenantroline)[86] Cp_3Y[87] $(CpCH_3)_3Y$[87]	O_2[85] O_3[85-86] H_2O[87]
La_2O_3	$La(thd)_3$[82-83] $[La(^iPr)NC(CH_3)N(^iPr)]$[84]	O_3[82-83] H_2O[84]
CeO_2	$Ce(thd)_4$[88-89] $Ce(thd)_3$(1,10-phenantroline)[89]	O_3[88-89]
Nd_2O_3	$Nd(thd)_3$[92]	O_3[92]
Sm_2O_3	$Sm(thd)_3$[94]	O_3[94]
Eu_2O_3	$Eu(thd)_3$[94]	O_3[94]
Gd_2O_3	$Gd(thd)_3$[94]	O_3[94]
Dy_2O_3	$Dy(thd)_3$[94]	O_3[94]
Ho_2O_3	$Ho(thd)_3$[94]	O_3[94]
Er_2O_3	$Er(thd)_3$[90,94]	O_3[90,94]
Tm_2O_3	$Tm(thd)_3$[94]	O_3[94]
Lu_2O_3	$\{[C_5H_4(SiMe_3)]_2LuCl\}_2$[93]	H_2O[93]
MgO	$Mg(thd)_4$[100] $[Mg_2(thd)_4]$[97] $MgEt_2$[98-99]	H_2O[97-99] O_3[100]
V_2O_5	$VO(O^iPr)_3$[95]	H_2O[95]

2.1 Film Growth

2.1.1 Aluminium Oxide, Al_2O_3

Al_2O_3 was among the first materials grown by ALD[101], selected ALD processes are presented in Table 2. Aluminium chloride has been used as the aluminium source with the following oxygen sources: H_2O[12–14], O_2[10–11,13] and several alcohols[13,15]. The growth rate depends on the reactor design, deposition temperature (100 – 800 ºC) and the oxygen source, it may also depend on the substrate material. It has typically been about 0.4 – 0.9 Å/cycle.[10,13–14]

Perhaps the most studied aluminium precursor is trimethylaluminium. It was first introduced by Higashi and Fleming[17] and has later on been studied by a number of groups using various oxygen sources: H_2O[17–20,24,I], H_2O_2[21,23,25], N_2O[25], $^{i}PrOH$[27] and O_3[26]. The highest growth rate obtained with the Me_3Al – H_2O process is about 1.2 Å/cycle. The growth rate obtained with H_2O_2 is of the same order. When $^{i}PrOH$[27] or O_3[26] were used as the oxygen source, the growth rate decreased to about 0.80 and 0.85 Å/cycle, respectively.

The above listed growth rates have been obtained at temperatures from 150 to 450 ºC. Recently, deposition of Al_2O_3 using Me_3Al and H_2O at temperatures as low as 33 ºC was reported.[102] The highest growth rates 1.33 Å/cycle were obtained at 100 – 125 ºC.

Dimethylaluminium chloride has been studied with water at 125 – 500 ºC.[28] The highest growth rate was 0.8 Å/cycle at 180 – 250 ºC. Another group has studied dimethylaluminium isopropoxide and water at 90 – 270 ºC obtaining a growth rate of 1.03 Å/cycle.[29]

Ritala et al.[16] have presented a new ALD process, where both precursors contain the same metal, hence both precursor pulses deposit metal into the films. The highest growth rate, 1.3 Å/cycle, was obtained for the Me_3Al – $Al(O^{i}Pr)_3$ process.

Table 2. Selected ALD processes for the deposition of Al_2O_3

Precursors/ Substrate	Deposition Temperature (ºC)	Growth rate (Å/cycle)	Crystallinity	Detected impurities (Method)	Refractive index	Ref.
$AlCl_3$-H_2O on glass and quartz	100 – 470	0.6 at 470 ºC	amorphous	not reported	1.71 at 470 ºC	12
$AlCl_3$-^{t}BuOH on glass	250 – 500	0.45 at 500 ºC	amorphous	Cl (XRF, chemical analysis)	not reported	15
$AlCl_3$-H_2O, O_2, alcohols	250 – 500	0.5 – 1.3	amorphous	not detected (Auger)	not reported	13
$AlCl_3$-H_2O on glass	500	0.4	amorphous	not reported	1.70	14
Me_3Al-H_2O on Si	100 – 500	1.1	amorphous	not reported	1.65 – 1.70	17
Me_3Al -H_2O Si	150 – 450	1.1	amorphous	not reported	1.65	18
Me_3Al -H_2O on Si	250 – 400	1.0	amorphous	H, C (SIMS)	1.64 – 1.68	19
Me_3Al -H_2O on Si	33 – 177	1.25	amorphous	H (FReS)	1.51 – 1.61	102
Me_3Al -H_2O_2 on various materials	150	1.13	amorphous	C not detected (XPS)	1.61	21
Me_3Al -^{i}PrOH on Si	250	0.8	amorphous	C (SIMS, XPS)	not reported	27
Me_3Al -O_3 on Si	350 – 400	0.85	amorphous	C (AES)	not reported	26
Me_2AlCl-H_2O on glass	125 – 500	0.8	amorphous	H, C, Cl (TOF-ERDA)	1.59 – 1.68	28
$Me_2Al(O^iPr)$ – H_2O on Si	100 – 270	1.06	amorphous	not detected (RBS)	not reported	29
$AlCl_3$-$Al(OEt)_3$ on Si	400	0.7	amorphous	C, H, Cl (TOF-ERDA)	not reported	16
$AlCl_3$-$Al(O^iPr)_3$ on Si	300	0.8	amorphous	C, H, Cl (TOF-ERDA)	not reported	16
Me_3Al -$Al(O^iPr)_3$ on Si	300	1.3	amorphous	C, H (TOF-ERDA)	not reported	16

The Al_2O_3 ALD films are amorphous as determined by XRD. The refractive index of a good quality film is usually 1.65 – 1.70.[14,17,19] The dielectric constant of Al_2O_3 films is relatively high: 7 – 9.[3] The films are not free of impurities. $AlCl_3$ leaves a chlorine residue, which usually decreases with increasing deposition temperature. Carbon and hydrogen are left in the films as impurities when Me_3Al is used as the Al precursor. Again, the amounts depend on the growth temperature, for example, Groner et al.[102] have reported 21.7 – 6.9 at.% of hydrogen detected in films grown at 33 – 177 ºC. The

amounts of carbon are reported to be lower than hydrogen, usually less than 1 at.%, especially at the higher growth temperatures.[14,19,26]

2.1.2 Titanium Dioxide, TiO_2

TiO_2 has been grown using halides and alkoxides as the metal source. H_2O[30–31,103,I,II] and H_2O_2[32–33] have been used as the oxygen source with $TiCl_4$. The highest growth rates obtained were 0.56[31] and 0.65[33] Å/cycle for H_2O and H_2O_2, respectively. The films were grown at temperatures 150 – 600 ºC. TiI_4 has been thoroughly studied using H_2O_2[34-35] and O_2[36–37] as the oxygen source. The growth rate for the TiI_4–H_2O_2 process was about the same as for the corresponding chloride: 0.64 Å/cycle. The films were grown at temperatures 250 – 490 ºC. The highest growth rate for the process using oxygen was 2.0 Å/cycle at 457 ºC.

Titanium alkoxides have also been used. The thermally most stable one is $Ti(OMe)_4$, the highest growth rates have been obtained with the methoxide. At 300 ºC, for example, the growth rates are about 0.5, 0.4 and 0.3 Å/cycle for $Ti(OMe)_4$[38], $Ti(OEt)_4$[41] and $Ti(O^iPr)_4$[40], respectively. The growth rate has been increased to 0.6 Å/cycle for both ethoxide and isopropoxide by using a larger water dose than what was used in Refs. 38 and 41.[I]

The TiO_2 films are crystalline and have either anatase or rutile structure usually depending on the deposition temperature.[31,34,II] The refractive index of these films is high, around 2.5.[31,36,38,40–41] A chlorine residue of about 2 at.% has been reported for the films grown at 150 ºC from $TiCl_4$; it decreased with increasing temperature being below the detection limit of RBS in the films grown at 500 ºC.[31] The films deposited using TiI_4 were essentially iodine free[34], except for the low deposition temperatures, where an iodine residue of about 0.2 at.% was left in the films.[36] The Ti alkoxide precursors leave hydrogen and carbon in the films, the carbon has been reported to be situated mostly on the film surface and in the substrate–film interface.[41] The hydrogen is in the bulk of the film and, again, the amount decreases as the deposition temperature is elevated.[38]

Table 3. Selected ALD processes for the deposition of TiO_2

Precursors/ Substrate	Deposition Temperature (ºC)	Growth rate (Å/cycle)	Crystallinity	Detected impurities	Refractive index	Ref.
$TiCl_4$-H_2O on glass, borosilicate	150 – 600	0.56	anatase, rutile	Cl (RBS)	2.4 – 2.6	31
$TiCl_4$-H_2O_2 on Si	340 – 490	0.65	anatase	not reported	2.6	33
TiI_4-H_2O_2 on glass, Si	250 – 490	0.6	anatase, rutile	H (TOF-ERDA)	2.70 – 2.75	34
TiI_4-O_2 on Si	230 – 460	1.0; 2.0 at 457 ºC	anatase, rutile	I (XPS)	2.2 – 2.5	36
$Ti(O^iEt)_4$-H_2O on glass	150 – 400	0.35	anatase	H, C (XPS, NRA)	2.5	41
$Ti(O^iPr)_4$-H_2O on glass	150 – 350	0.3	anatase	H (NRA)	2.5	40
$Ti(OMe)_4$-H_2O	200 – 400	0.65	anatase	H, C (TOF-ERDA)	2.5	38

2.1.3 Zirconium Dioxide, ZrO_2

Ritala et al.[42] were the first to grow ZrO_2 by ALD from $ZrCl_4$ and H_2O. The growth rate obtained at 500 ºC was 0.53 Å/cycle. This was increased to 0.75 Å/cycle with a larger water dose than in Ref. 42.[I] Recently films grown with this process have been thoroughly studied by several groups.[104–109] In the case of ZrI_4, H_2O_2 was used as the oxygen source.[44] The films were grown at 250 – 500 ºC and the highest growth rate (1.25 Å/cycle) was achieved already at 275 ºC.

Several organometallic and metal organic compounds have been used as the metal precursor. Thin films from $Zr(O^tBu)_4$ have been grown using H_2O[45] and O_2[46]. Saturative growth could not be achieved because of thermal decomposition of $Zr(O^tBu)_4$: the growth rate increased with increasing Zr precursor pulse length. In an attempt to stabilise the compound, a donor-functionalised ligand, dimethylaminoalkoxide, has been added and films were grown from $Zr(O^tBu)_2(dmae)_2$[V,VI], $Zr(O^iPr)_2(dmae)_2$ and $Zr(dmae)_4$[VI] and water. Thermal decomposition was still observed during the ALD growth.

Ozone has successfully been used as an oxygen source also in the case of ZrO_2. It has been used with $Zr(thd)_4$, $Cp_2Zr(Me)_2$ and Cp_2ZrCl_2.[47] The growth rate was very moderate for the β-diketonate: 0.24 Å/cycle at 375 ºC, at higher temperatures thermal decomposition caused thickness nonuniformity. The cyclopentadienyl complexes also started to decompose at temperatures above 350 ºC. Below that temperature a constant growth rate of 0.55 and 0.53 Å/cycle was obtained for $Cp_2Zr(Me)_2$ and Cp_2ZrCl_2, respectively. $Cp_2Zr(Me)_2$ has also been used with H_2O, but in that case the growth rate was lower: 0.43 Å/cycle.[48]

ZrO_2 has been grown at 50 – 500 ºC using zirconium alkylamides and water with good growth rate: 0.96 Å/cycle.[50] The films were smooth and conformal.

The ZrO_2 films were crystalline with a dielectric constant of 20[3]. The refractive index was quite high, about 2.2 for the films grown using $ZrCl_4$. These films contained some hydrogen, about 0.4 at.%, while the chlorine content was below the detection limit of

RBS, i.e. it was below 0.5 at.%.[42] A deposition temperature dependent iodine residue was found in the films grown using ZrI_4, 1.3 – 0.8 at.% for temperature range 250 – 350 ºC.[44] A substantial amount of hydrogen and carbon impurities has been detected in the films grown using Zr alkoxides[45] and Zr aminoalkoxides[V,VI], for example, about 23 at.% of hydrogen and 6 at.% of carbon was detected in the films grown from $Zr(O^tBu)_4$ at 175 ºC.[45] Less impurities have been observed in the films grown from $Zr(thd)_4$: only 0.2 and 0.3 at.% of carbon and hydrogen, respectively.[47] The cyclopentadienyl complexes[47–48] also yield smaller impurity amounts in the films than the alkoxides. For example, Cp_2ZrMe_2 leaves only about a 0.5-at.% carbon and hydrogen residue.[47] The films grown from aminoalkyls are reported to contain less than 1 at.% of carbon and about 0.25 at.% nitrogen as impurities.[50]

Table 4. Selected ALD processes for the deposition of ZrO_2

Precursors/ Substrate	Deposition Temperature (°C)	Growth rate (Å/cycle)	Crystallinity	Detected impurities	Refractive index	Ref.
$ZrCl_4$-H_2O on glass	500	0.53	nearly amorphous	Cl not detected (RBS), H (NRA)	2.2	42
$ZrCl_4$-H_2O_2 on Si, silica	180 – 600	1.35	cubic, tetragonal, monoclinic	Cl (EPMA)	2.05	43
ZrI_4-H_2O_2 on Si, quartz	250 – 500	1.25	cubic, tetragonal, monoclinic	I (XPS)	2.05 – 2.25	44
$Zr(O^tBu)_4$-H_2O on glass, borosilicate	150 – 300	0 – 1.9	nanocrystalline	H, C (TOF-ERDA)	1.9	45
$Zr(dmae)_2(O^tBu)_4$-H_2O on glass, borosilicate	190 – 340	0.58 – 1.32	nanocrystalline	H, C, N (TOF-ERDA)	2.08	V,VI
$Zr(dmae)_2(O^iPr)_4$-H_2O on glass, borosilicate	190 – 340	0.70 – 1.48	nanocrystalline	H, C, N (TOF-ERDA)	2.07	VI
$Zr(dmae)_4$-H_2O on glass, borosilicate	190 – 340	0.58 – 1.08	nanocrystalline	H, C, N (TOF-ERDA)	2.00	VI
$Zr(thd)_4$-O_3 on glass	275 – 500	0.24	weakly crystalline	H, C, F (TOF-ERDA)	not reported	47
Cp_2ZrMe_2-O_3 on glass	250 – 500	0.55	weakly crystalline	H, C, F (TOF-ERDA)	not reported	47
Cp_2ZrCl_2-O_3 on glass	200 – 500	0.53	weakly crystalline	H, C, F (TOF-ERDA)	not reported	47
Cp_2ZrMe_2-H_2O on Si	200 – 500	0.43	polycrystalline	H, C (TOF-ERDA)	not reported	48
$Zr(NMe_2)_4$-H_2O $Zr(NMeEt)_4$-H_2O $Zr(NEt_2)_4$-H_2O on Si	50 – 500	0.96	not reported	N, C (RBS)	2.10	50
$ZrCl_2[N(SiMe_3)_2]_2$ – H_2O	150 – 350	1.6	amorphous	Si (RBS)	1.6-1.7	51

2.2. *In situ* Studies on ALD Dielectric Oxide Processes

Table 5 summarises the *in situ* reaction mechanism studies conducted on ALD dielectric oxide processes using QCM or/and QMS. Reaction mechanism studies carried out on selected Al_2O_3, TiO_2 and ZrO_2 growth processes are discussed in more detail, except for $Me_3Al–H_2O$ and $TiCl_4–H_2O$ which are discussed in chapters 4.1.1 and 4.2.4, respectively.

The *in situ* characterisation methods that can be applied to follow the growth process in flow-type ALD reactors, which are industrially the most important ones and have been in use also in this thesis, can be divided to optical methods, microgravimetric methods and mass spectrometry. The optical methods that have been applied are fourier transform infrared (FTIR) spectroscopy[72,110] and incremental dielectric reflection (IDR)[111–115]. FTIR has been used to study $Me_3Al–H_2O$[72,110] and $SiCl_4–H_2O$[72] processes and IDR to study $TiCl_4–H_2O$ process.

The optical methods give information about the surface. Another method which characterises the surface during the film growth is quartz crystal microbalance (QCM). It has been quite widely used to study ALD film growth *in situ*; selected publications are presented in Table 5.

Mass spectrometry is the method with which information about the species and reaction products in gas phase can be obtained. The QMS data reveal the gaseous products released in the surface reactions. By combining the QMS measurements with QCM , it is possible to study both the amount of material deposited on the surface and the gaseous reaction by-products. Selected studies where QMS has been utilized in the *in situ* characterisation of ALD processes are presented in Table 5.

$Ti(OEt)_4–H_2O$ process has been studied with QCM[126] and with QCM–QMS combination[127]. The growth has been suggested to proceed via ligand exchange reactions where the main reaction by-product is EtOH.[41] This can be described by Reactions 1 and 2 where s denotes a surface species.

$$–OH\ (s) + Ti(OEt)_4\ (g) \rightarrow (–O–)Ti(OEt)_3\ (s) + EtOH\ (g) \qquad (1)$$

$$(\text{–O–})\text{Ti(OEt)}_3\ (s) + 2\ \text{H}_2\text{O}\ (g) \rightarrow (\text{–O–})_2\text{Ti(OH)}\ (s) + 3\ \text{EtOH}\ (g) \qquad (2)$$

In the first step (1), the incoming $Ti(OEt)_4$ reacts with the OH groups on the surface and part of the –OEt ligands are released as EtOH. In the second step (2), the subsequent water pulse releases the rest of the ligands and the surface becomes OH terminated again.

The QCM study[126] revealed that at 225 – 250 ºC less than one ligand was released during the $Ti(OEt)_4$ adsorption. The QMS results[127], in turn, showed that most of the ligands were released during the water pulse, which suggested that the film would grow via molecular adsorption of $Ti(OEt)_4$ (Reactions 3 and 4).

$$\text{Ti(OEt)}_4\ (g) \rightarrow \text{Ti(OEt)}_4\ (s) \qquad (3)$$

$$\text{Ti(OEt)}_4\ (s) + 2\ \text{H}_2\text{O}\ (g) \rightarrow \text{TiO}_2\ (s) + 4\ \text{EtOH}\ (g) \qquad (4)$$

This perhaps is not the whole truth though, since it was also shown that the ethanol produced in reaction (1) could adsorb back onto the surface and then be released during the following water pulse. This increases the amount of ethanol released during the water pulse and complicates the interpretation of the QMS data.

$Ti(O^iPr)_4 – H_2O$ ALD process has been studied *in situ* with QCM[128] and QCM–QMS combination[129]. It was observed that about half of the isopropoxo ligands are released during the $Ti(O^iPr)_4$ pulse and the other half during the water pulse.[129] The growth could be described with the mechanism presented in Reactions 5 and 6.

$$2\ \text{–OH}\ (s) + \text{Ti(O}^i\text{Pr)}_4\ (g) \rightarrow (\text{–O–})_2\text{Ti(O}^i\text{Pr)}_2\ (s) + 2\ ^i\text{PrOH}\ (g) \qquad (5)$$

$$(\text{–O–})_2\text{Ti(O}^i\text{Pr)}_2\ (s) + 2\ \text{H}_2\text{O}\ (g) \rightarrow (\text{–O–})_2\text{Ti(OH)}_2\ (s) + 2\ ^i\text{PrOH}\ (g) \qquad (6)$$

The incoming $Ti(O^iPr)_4$ reacts with two OH groups at temperatures 150 – 275 ºC, at temperatures above that the dehydroxylation of the surface begins to affect the mechanism which starts to approach the one where only a single isopropoxide ligand is released during the titanium precursor pulse. (c.f. Reactions 1 and 2)

Table 5. Selected ALD processes studied *in situ*.

D_2O has been in use instead of H_2O in the case of QMS studies.

Material	Process	Method
Al_2O_3	$AlCl_3 + H_2O$	QCM [116]
	$Me_3Al + H_2O/D_2O$	QMS [117–118] QCM+QMS [119] QCM [120]
	$Me_3Al + H_2O_2$	QCM [22]
TiO_2	$TiCl_4 + H_2O/ D_2O$	QCM [121–123] QCM + QMS [IV]
	$TiI_4 + H_2O_2$	QCM [36,124–125]
	$Ti(OEt)_4 + H_2O/ D_2O$	QCM [126] QMS [127]
	$Ti(O^iPr)_4 + H_2O/ D_2O$	QMS [117] QCM [128] QCM + QMS [129]
ZrO_2	$ZrCl_4 + H_2O/ D_2O$	QCM [43] QCM + QMS [130]
	$ZrI_4 + H_2O$	QCM [44]
Ta_2O_5	$TaCl_5 + H_2O$	QCM [64,131–133]
	$TaI_5 + H_2O$	QCM [68]
	$Ta(OEt)_5 + H_2O/ D_2O$	QCM [134] QMS [117,127]
HfO_2	$HfCl_4 + H_2O$	QCM [135]
	$HfI_4 + H_2O$	QCM [136]
Nb_2O_5	$Nb(OEt)_5 + D_2O$	QMS [117,127]
V_2O_5	$VO(O^iPr)_3 + H_2O$	QCM [99]

$ZiCl_4 – H_2O$ process has been studied with QCM[43] and QCM–QMS[130]. The growth mechanism is presented in Reactions 7 and 8.

$$2 –OH (s) + ZrCl_4 (g) \rightarrow (–O–)_2ZrCl_2 (s) + 2 HCl (g) \quad (7)$$

$$(–O–)_2ZrCl_2 (s) + 2 H_2O (g) \rightarrow (–O–)_2Zr(OH)_2 (s) + 2 HCl (g) \quad (8)$$

At temperatures of 250 – 375 ºC two ligands are released during the adsorption of the zirconium precursor, while at temperatures above that the decreasing OH coverage of the surface begins to influence the mechanism and less ligands are released during the $ZrCl_4$ pulse.[130]

3. Experimental

3.1 Film Growth

A commercial F-120 flow-type reactor manufactured by ASM Microchemistry Ltd.[2] was used in the film growth experiments. The reactor pressure during the deposition was about 10 mbar. Nitrogen (99.999%) was used as a carrier and purging gas. The films were grown on 5 × 5 cm^2 substrates, either soda lime or borosilicate glass, or stainless steel (for the corrosion studies).

Depending on their vapour pressure the precursors were evaporated either from external or internal sources. The pulsing of reactants was accomplished by solenoid valves; needle valves were used to control the dose of some of the externally evaporated sources.

3.2 Film Characterisation

The thickness and refractive index of the films were evaluated by fitting transmittance spectra according to Ylilammi and Ranta-aho.[137] The thickness of the films on stainless steel was determined from the maxima and minima of the reflectance spectra using the optical parameters evaluated for the corresponding films on glass, i.e. those deposited in the same process. The spectra were measured with a Hitachi U-2000 spectrophotometer. The refractive indices are given for λ=580 nm. The crystal structure and orientation of the films were studied with a Philips MPD 1880 powder XRD diffractometer using Cu K_α radiation. The chemical composition of the films was studied by time-of-flight elastic-recoil-detection analysis (TOF-ERDA)[138] and nuclear resonance broadening (NRB)[139].

3.3. Reaction Mechanism Studies

The *in situ* studies were carried out in a set-up comprising a QMS and a QCM integrated to a specially modified F-120 reactor (Fig. 1) equipped with an enlarged reaction chamber. The pressure in the ALD reaction chamber was about 2 mbar, the

pressure reduction from the reactor to the QMS chamber was accomplished through an orifice (20 – 200 μm of diameter). The gas composition was measured with a Hiden HAL/3F 501 RC QMS, which has a mass range of 1 – 510 amu. A Faraday cup detector was used; the ionisation energy was 70 eV. The mass balance studies were made using a Maxtek TM 400 QCM. The operating frequency of the crystal was 6 MHz; the sampling rate was 20 times per second. The reaction chamber was filled with glass substrates, the total surface area being about 3500 cm^2 to maximise the amount of reaction by-products. D_2O was used as the oxygen source instead of H_2O to better distinguish the reaction by-products from the species formed in the ionisator.

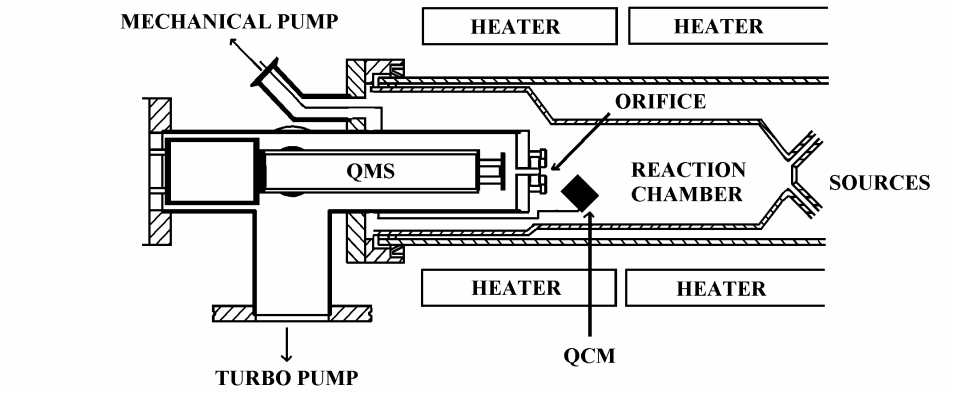

Figure 1. A schematic view of the reactor used in the reaction mechanism studies. The precursors are transported with the carrier gas to the reaction chamber from the right and are pumped by the mechanical pump. A small part of the total flow is pumped by the turbomolecular pump through the sampling orifice and the QMS chamber.

QMS data Figure 2a shows how the data recorded by the QMS typically looks like. As can be seen, weak signals are often observed even when no exchange reactions should take place, i.e. when only one precursor is repeatedly pulsed. This phenomenon can not be explained thoroughly but several reasons have been suggested[140]: possible rearrangement reactions during ionisation, condensation of the metal precursor to the cooler end of the reactor tube behind the QMS, or pressure change during the precursor pulse which could affect the observed signal. This background signal is subtracted from the signal observed for the same precursor during the ALD process.

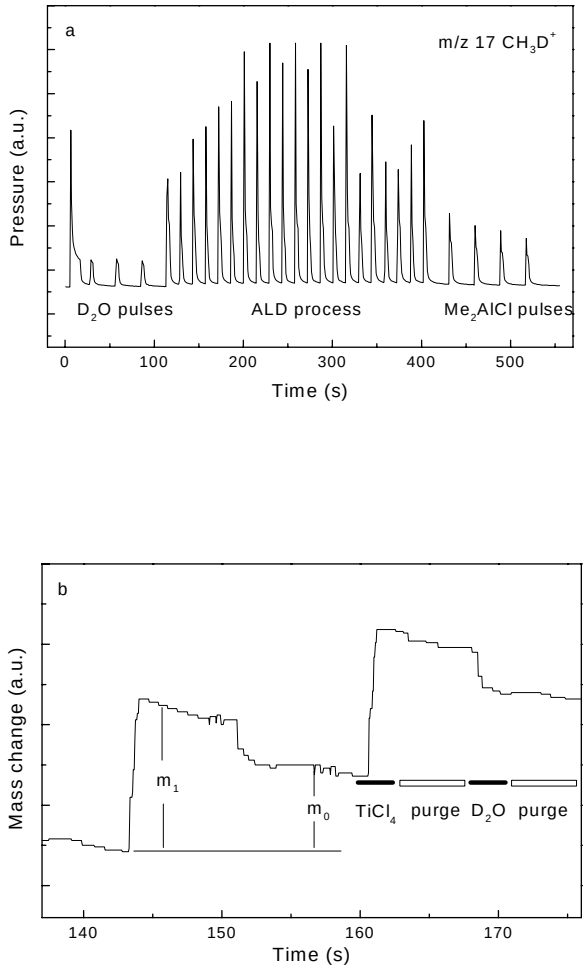

Figure 2. a) Data recorded with the QMS during the whole pulsing sequence used in studying the Me_2AlCl–D_2O process. b) Data recorded with the QCM during two complete ALD cycles of the $TiCl_4$–D_2O process.

QCM data A part of the QCM signal recorded during an ALD process is presented in Figure 2b. During the metal precursor pulse the weight increases because of the adsorption of $–ML_{x-n}$ species. This mass increment during the metal precursor pulse is marked with m_1. The water pulse causes a decrease in the weight as the –L ligands are replaced by lighter –OH groups or oxide ions. The mass increment after a complete ALD cycle is marked with m_0 and it is directly related to the growth rate. Because an oxide MO_y is deposited, m_0 corresponds to the molar mass of MO_y, while m_1 corresponds to the adsorbate ML_{x-n} formed during the metal pulse. Therefore, the ratio of these adsorbates can be used to calculate how many ligands are released during the metal precursor and water pulses:

$$\frac{m_0}{m_1} = \frac{M(MO_y)}{M(ML_x) - nM(HL)} \quad (9)$$

In Equation 9, M denotes metal, L is a ligand bound to the metal and M(i) is the molar mass of the species i and n is the number of ligands released during the metal precursor pulse:

$$n\ –OH\ (s) + ML_x\ (g) \rightarrow (–O–)_nML_{x-n}\ (s) + n\ HL\ (g) \quad (10)$$

(according to Rahtu PhD thesis[140])

The *n* value can be calculated also from the QMS data as follows: the amount of reaction by-product HL released during the metal precursor pulse is divided by the total amount of the same by-product (the amount released during the metal precursor pulse plus the amount released during the water pulse) and then multiplied by the total number of ligands attached to the metal (x).

4. Results and Discussion

4.1 Effect of Water Dose on the ALD Growth Rate [I]

Background As presented previously, ALD is based on alternate saturative surface reactions. The incoming precursor molecules chemisorb or react with surface groups and saturation of the surface is reached only when all the reactive sites are used. In an ideal case, a monolayer is formed after each precursor pulse. However, often the deposition rate is less than a monolayer because of limited density of the surface groups or sterical reasons. These factors often depend on deposition temperature.

In the ALD growth of oxide films using water as the oxygen source, the important surface sites are hydroxyl groups.[18,141–142] The film growth starts with the incoming metal precursor reacting with the OH covered surface.

$$x\ –OH\ (s) + ML_n\ (g) \rightarrow (–O–)_xML_{n-x}\ (s) + xHL\ (g) \quad (11)$$

The subsequent water pulse reacts then with the remaining ligands recreating the OH coverage onto the surface.

$$(–O–)_xML_{n-x}\ (s) + ½(n-x)\ H_2O\ (g) \rightarrow (–O–)_xM(OH)_{n-x}\ (s) + (n-x)\ HL\ (g) \quad (12)$$

In Reactions 11 and 12 s denotes a surface species, M metal and L ligand bound to the metal.

There are two kinds of OH groups on the surface: terminal and bridging between two or more cations.[143] The terminal OH groups can be either adjacent and possibly hydrogen bonded with each other or isolated. The various types of hydroxyl groups are depicted in Figure 3.

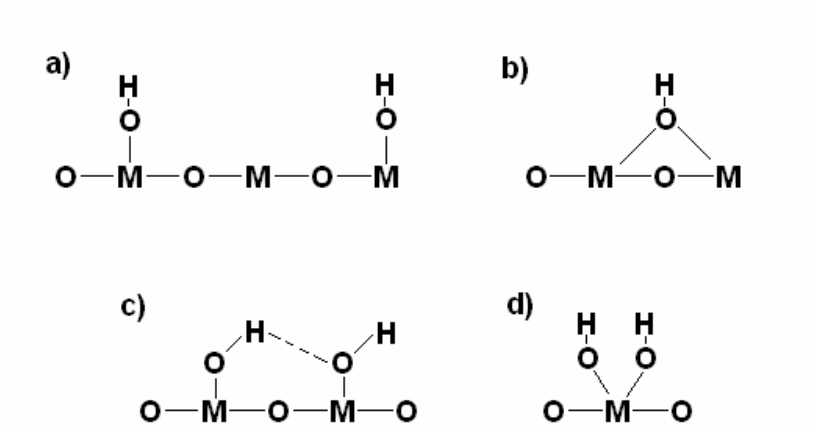

Figure 3. Different types of hydroxyl groups on oxide surfaces: a) isolated terminal, b) bridging between two cations, c) hydrogen bonded terminal, d) geminal hydroxyl group. (schematics after ref. 140)

The OH groups are not stable at elevated temperatures: they may condense with each other causing dehydroxylation of the surface (Fig. 4a). This dehydroxylation increases with increasing temperature causing decrease of the surface hydroxyl group density (Fig. 5) Especially the hydrogen bonded hydroxyls are favourable for dehydroxylation. Rehydroxylation of the surface is also possible by dissociative chemisorption of water molecules (Fig. 4b and c).

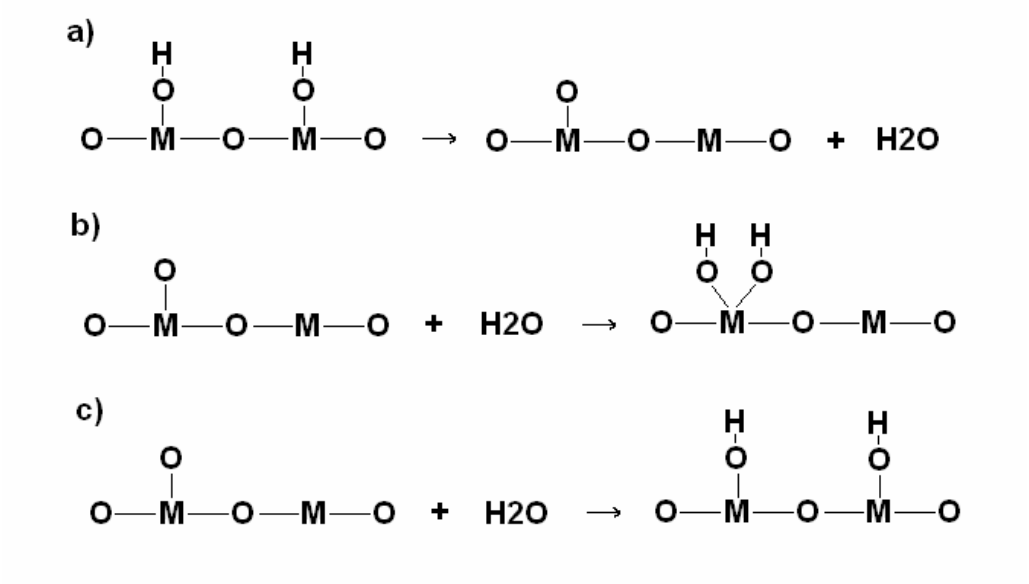

Figure 4. Reaction a depicts dehydroxylation of the surface. The reverse of that reaction, rehydroxylation is depicted in b and c.

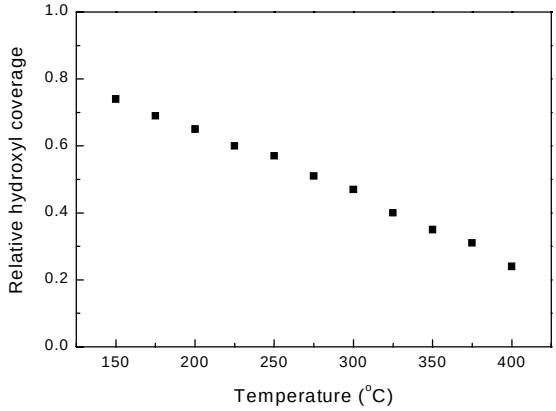

Figure 5. The relative hydroxyl coverage of amorphous Al_2O_3 surface as a function of temperature.[144]

It has been thought that the only growth rate limiting factor is the number of reactive surface sites if the precursor dose is high enough for the saturation. Surprisingly, the growth rate can be increased by further increasing the precursor dose, i.e. precursor concentration in the gas phase.[145,I]

4.1.1 Me_3Al – H_2O process

The ALD growth of aluminium oxide from trimethylaluminium and water has been widely studied.[17–18,25,146,I] A reaction mechanism has been proposed for the film growth[118–119,147]: the incoming Me_3Al reacts with the surface hydroxyls liberating methane, during the second half reaction water releases the rest of the methyl groups producing a hydroxyl terminated surface again.

$$n\ –OH\ (s) + Me_3Al\ (g) \rightarrow (–O–)_nAlMe_{3-n}\ (s) + n\ CH_4\ (g) \quad (13)$$

$$(–O–)_nAlMe_{3-n}\ (s) + 1.5\ H_2O\ (g) \rightarrow (–O–)_{1.5}Al(OH)_n\ (s) + (3-n)\ CH_4\ (g) \quad (14)$$

Increasing the OH density on the surface increases the adsorption of Me_3Al and hence the growth rate. Indeed, it was observed that the growth rate could be increased by increasing the water dose. A large enough water dose is needed to saturate also the coordinatively unsaturated surface (c.u.s.) aluminium and oxygen sites.[119] Two kinds of reactions are suggested to take place during the water pulse and reaction 16 is the one which is most affected by the increased water dose.[119]

$$Al–CH_3\ (s) + H_2O\ (g) \rightarrow Al–OH\ (s) + CH_4\ (g) \quad (15)$$

$$Al–O–Al\ (s) + H_2O\ (g) \rightarrow 2\ Al–OH\ (s) \quad (16)$$

The water dose was varied between 3×10^{-6} and 1×10^{-4} g/cycle. At first, the growth rate increased rapidly but finally saturated to a level of about 1.0 Å/cycle when the water dose was about 6×10^{-5} g/cycle (Fig. 6). After that point the increment in the water dose could no longer increase the number of OH groups on the surface and hence did not any more increase the growth rate.

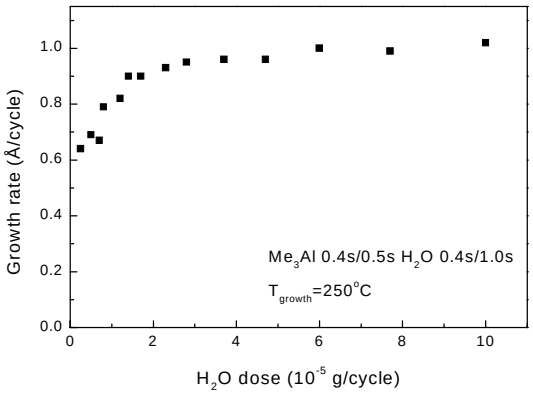

Figure 6. The growth rate of Al_2O_3 determined for various water doses.

When the water pulse was varied from 0.5 to 3.5 s the growth saturated with both the above mentioned water doses but to a different level: at 0.95 Å/cycle with the small dose and at 1.16 Å/cycle with the large dose (Fig. 7). This shows that the ALD growth rate is not always independent of the precursor dose even when it is above the limit for saturating the surface reactions. The small and large water doses refer to 8×10^{-6} and 2×10^{-4} g/s water flow rates, respectively.

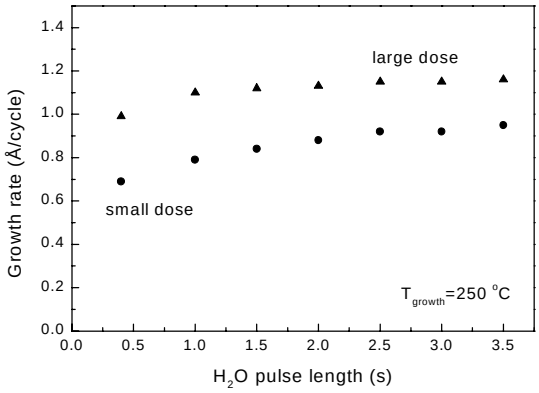

Figure 7. The growth rate for small (8×10^{-6} g/s) and large (2×10^{-4} g/s) water flow rate.

The growth rate saturated to a higher level with the large water dose than with the small dose at all deposition temperatures (150 – 500 ºC). At the higher temperatures the saturation levels became closer to each other and at 500 ºC they almost met. This means that at high temperatures dehydroxylation is so rapid that it cannot be compensated even with a very large water dose.

The large H_2O doses did not affect the quality of the films. The refractive indices varied from 1.63 to 1.67 between 150 and 500 ºC, respectively, but there was no difference between the small and large water dose. Films grown at 250 ºC were analysed for residual impurities by TOF-ERDA. No significant difference was observed between the samples grown using the small and large water doses: the hydrogen contents were 1.0 and 1.1 at.%, respectively. The carbon content was less than 0.2 at.%.

4.1.2 Other Oxide Processes

A slight or even a large increase in the growth rate compared to the earlier published ones was obtained for all the ALD processes that were studied (Fig. 8) when a higher water dose was used. Below in text, small and large water doses refer to water flow rates of 8×10^{-6} and 2×10^{-4} g/s, respectively.

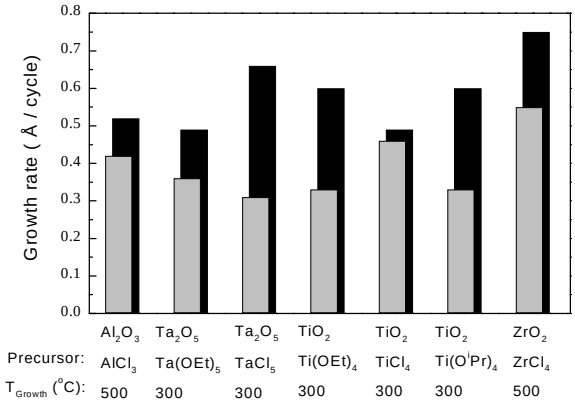

Figure 8. The effect of the small (8×10^{-6} g/s) and large (2×10^{-4} g/s) water flow rate on the oxide growth rate. The grey and black columns present the growth rates obtained with the small and large flow rates, respectively.

Al_2O_3 A somewhat increased growth rate from 0.42 to 0.52 Å/cycle was obtained for the $AlCl_3$ – H_2O process when the water dose was varied. The growth rates obtained earlier were of the order of 0.40 Å/cycle[14], the refractive index (1.70) was higher than what was evaluated for the films in the present study for both water doses (1.66).

ZrO_2 A growth rate of 0.53 Å/cycle has been reported earlier for the $ZrCl_4$–H_2O ALD process.[42] In this study, that growth rate was obtained already with the small water dose, and a higher growth rate of 0.75 Å/cycle was achieved with the large water dose. The refractive indices were 2.2 and 2.3 for the small and large dose, respectively. These are comparable with the 2.2 reported earlier.[42] Only rather weak reflections were observed in the XRD measurements, which is in accordance with the earlier observations.[42]

TiO_2 In the case of the $TiCl_4$ – H_2O process, the larger water dose affected the growth rate only slightly: it increased from 0.46 to 0.49 Å/cycle. The refractive index of the film grown with the larger water dose was higher than the one grown with the smaller dose: 2.55 vs. 2.40, respectively. The higher refractive index indicates better film quality, the most likely explanation being that the larger water dose effectively removes the chloride ligands. XRD showed no major differences in the films: both films showed weak reflections of the anatase phase.

The increased water dose had a significant effect on the growth rate in the case of the other Ti precursors, $Ti(O^iPr)_4$ and $Ti(OEt)_4$: the growth rate was increased from 0.33 to 0.60 Å/cycle. The low growth rate is most likely caused by steric reasons as the ethoxo and isopropoxo ligands take up a good deal of room on the surface. The larger water amount removes more ligands from the adsorbed Ti precursor. The effective removal of the ligands is also supported by the compositional analysis (by TOF-ERDA), which showed that there is only about 0.1 at.% of hydrogen and less than 0.2 at.% of carbon residues in the films.

Ta_2O_5 The growth rate for the $TaCl_5$ – H_2O process was more than doubled from 0.31 to 0.66 Å/cycle when the water dose was increased. It has been suggested that as the H_2O releases the chloride ligands, it either recreates OH groups on the surface or creates a bridging oxygen.[133] These oxygen bridges are less reactive than OH groups

and hence decrease the growth rate. It is likely that the large water dose enhances the recreation of surface OH groups.

Results obtained with the other Ta precursor, $Ta(OEt)_5$, were 0.36 and 0.49 Å/cycle for small and large water dose, respectively. These films were analysed by TOF-ERDA for carbon and hydrogen: there were more impurities in the film grown using the smaller water dose than with the large dose: 1.1 vs. 0.3 at.% of carbon and 1.5 vs. 0.6 at.% of hydrogen. The diminished amount of impurities suggests that the ethoxo ligands are removed more effectively with the large water dose which is most probably also the reason for the increased growth rate.

4.2. Al_2O_3 and TiO_2 [II]

The characteristics of ALD make it a tempting technique also for depositing corrosion protection coatings. In this respect, the most important advantages of ALD are excellent conformality both in macroscopic (complex shaped objects) and microscopic (surface roughness and irregularities) scales, and the high quality of the films prepared, particularly their dense, pinhole-free structures. Yet another advantageous feature of ALD is that since the substrate-film interface is formed via saturative chemical reactions, good adhesion may be expected. Together with the barrier properties of the coating, adhesion has the largest impact on the corrosion protection of metallic substrates by inorganic coatings, the overall corrosion resistance being determined in the first place by adhesion.

Ceramic corrosion protection coatings have typically thicknesses of at least one micron. For depositing such thick coatings, ALD appears to be too slow. However, because of its superior conformality and high film density, ALD shows a promise to protect the underlying objects already with thinner films. The film materials chosen for this corrosion protection study were Al_2O_3 and TiO_2 because these processes were well established[17,21,31,72], and they could be carried out at low temperatures which is considered crucial to avoid cracking due to thermal stresses.

The growth and characterisation of Al_2O_3 and TiO_2 films is discussed first and then the corrosion protection properties of these films are addressed briefly. Some

unpublished results are included. Finally, the reaction mechanisms in two ALD processes are examined: Me_2AlCl–D_2O and $TiCl_4$–D_2O.

4.2.1. Film Growth and Characterisation

Al_2O_3 The films were deposited from Me_3Al and H_2O at a temperature range of 150 – 400 °C. Figure 9 shows the growth rates on glass and stainless steel. Both plots follow the same trend; the growth rate seems to be independent of temperature between 200 and 350 °C. The slight decrease in the growth rate at 400 °C is most possibly caused by dehydroxylation of the surface, but partial decomposition of Me_3Al already before it reaches the substrate may also affect the growth rate[148]. At 150 °C, the kinetics of the surface reactions is probably the growth rate limiting factor[148]. The thicknesses of the films grown were between 250 and 310 nm.

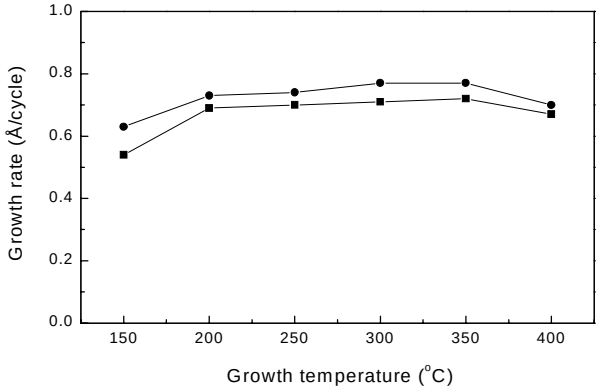

Figure 9. Dependence of Al_2O_3 growth rate on temperature. (■ = glass substrate, ● = steel substrate).

The chemical composition of the films was studied by TOF-ERDA and NRB. The results of these analyses are depicted in Figs. 10-12. There was a small carbon residue in all the films but it decreased from 0.8 at.% to about 0.2 at.% with increasing temperature (Fig. 10). Due to adsorbed hydrocarbons the carbon concentration shows a peak at the film surface but is otherwise evenly distributed (Fig. 11). The hydrogen content is the highest in the film grown at 150 °C and it decreases as the growth temperature is raised (Figs. 10 and 12). The lowest hydrogen contents were close to

the detection limit of the NRB technique. The high hydrogen peak at the surface (Fig. 12) is due to adsorbed water and hydrocarbons. The large hydrogen contents in the films grown at low temperatures (Fig. 10) imply that some hydroxyl groups are left in the films because of incomplete reactions. On the other hand, some -CH_x residues may also exist in these films since they have the highest carbon contents (Fig. 10). The refractive index measured at λ = 580 nm correlates with the hydrogen contents: it increases from 1.62 to 1.67 with the increasing deposition temperature. Low hydrogen residue and high refractive index indicate good film quality.

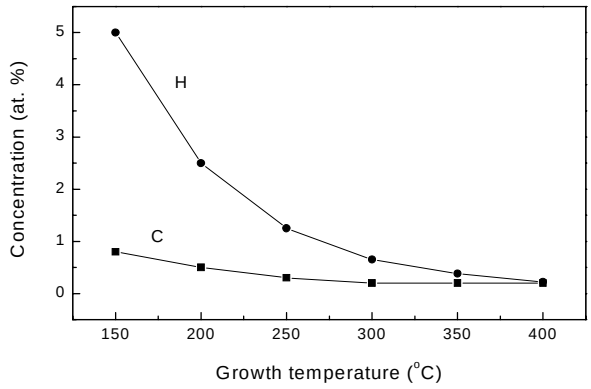

Figure 10. Temperature dependencies of C and H residual contents in Al_2O_3 films grown on glass measured by TOF-ERDA and NRB.

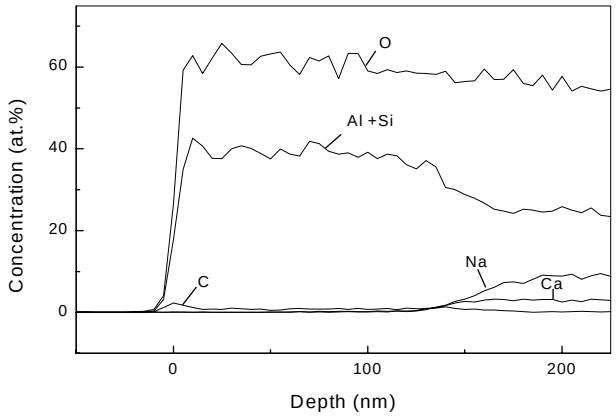

Figure 11. Element depth profiles of an Al_2O_3 film deposited at 150 °C as analysed by TOF-ERDA.

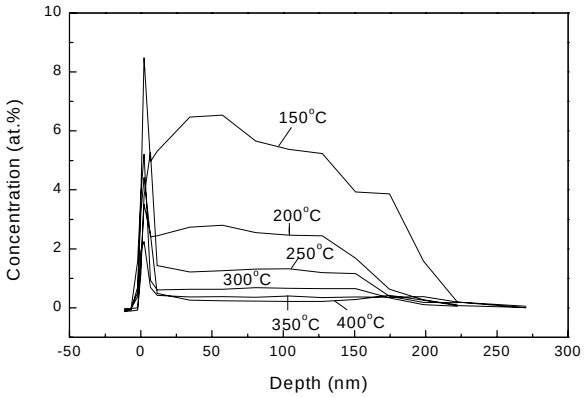

Figure 12. Hydrogen depth profiles in Al_2O_3 films grown at different temperatures as analysed by NRB.

Aluminium oxide is an amphoteric compound; i.e. it is readily soluble in both acids and alkalis. Etching tests with NaOH and H_3PO_4 were made to examine the chemical stability of the films, which was found to be growth temperature dependent getting worse with decreasing temperature (Fig. 13). The etching rates correlate nearly linearly with the hydrogen contents (Fig. 14) and inversely with refractive index thereby relating the chemical stability to CH_x or OH (or both) residues and film density. The films dissolve slowly over a time period of 8 weeks also into the 3.5 w-% NaCl solution used in the corrosion tests. Therefore, aluminium oxide can be used as a protective coating only in rather neutral conditions. On the other hand, the dissolution rate into acids and bases can be used as a measure of the film quality.

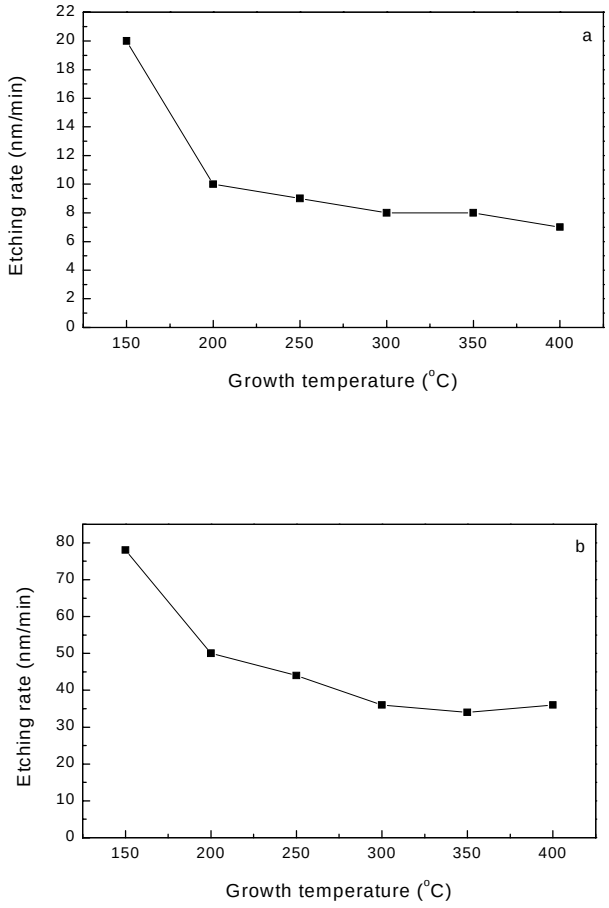

Figure 13. The etching rate for Al_2O_3 films at 60 °C. The etching solution was (a) 7 M H_3PO_4 and (b) 0.1 M NaOH.

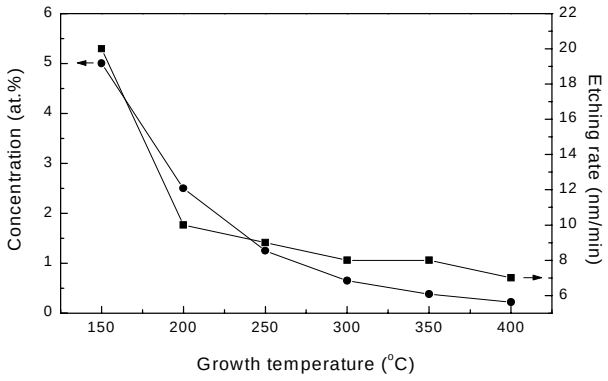

Figure 14. The hydrogen concentration determined by TOF-ERDA and the etching rate (7 M H_3PO_4) correlate nearly linearly.

TiO_2 The TiO_2 films were deposited using $TiCl_4$ and H_2O at a temperature range of 150 – 400 °C. The growth rates of the films are depicted in Fig. 15. There seems to be a rather large difference in the growth rates on glass and steel at 250 °C. The lower growth rate achieved at 150 °C is again most probably due to kinetic reasons. The thicknesses of the films were between 170 and 290 nm.

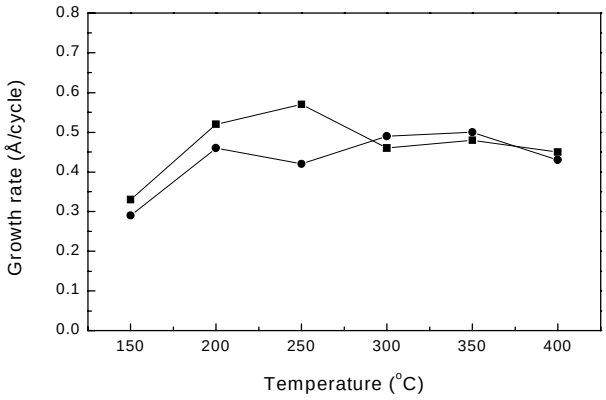

Figure 15. Dependence of TiO_2 growth rate on temperature (■ = glass substrate, ● = steel substrate).

The XRD patterns of TiO_2 films deposited onto stainless steel at 150 – 400 °C are shown in Fig. 16. The film grown at 150 °C was amorphous; the other films were crystalline having either anatase (below 300 °C) or rutile (above 300°C) structure depending on the deposition temperature.

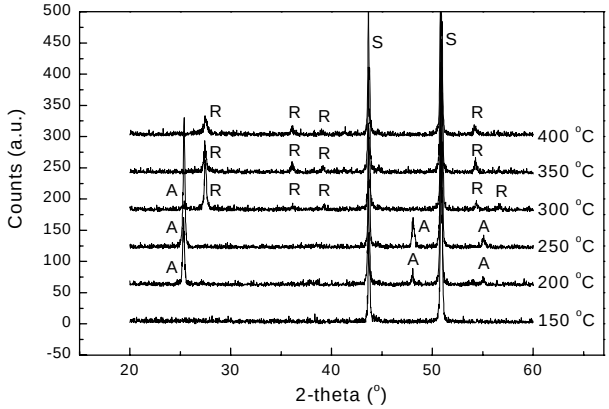

Figure 16. XRD patterns for TiO_2 films on stainless steel substrates deposited at 150–400 °C.

The chemical composition of the film grown at 150 °C as determined by TOF-ERDA is depicted in Fig. 17. The films grown at 150 and 200 °C had a small carbon residue content of about 2 at.%; in the rest of the samples the carbon content was very low, near the detection limit of the TOF-ERDA method. Anyhow, the residual carbon is mostly due to adsorbed hydrocarbons and is concentrated near the surface. An evenly distributed chlorine concentration of about 2 at. % was detected in the film grown at 150 °C. The chlorine content decreases with increasing temperature. Hydrogen contents were found to have maxima both at the outer surface and at the film-substrate interface (Fig. 18). The maxima are due to water and hydrocarbons adsorbed on the substrate surface before film deposition and on the film after the deposition. The hydrogen residue of the film-substrate interface decreases with increasing temperature suggesting that it is mostly due to adsorbed water that desorbs at higher temperatures. In the bulk of the films the hydrogen contents are low, below 0.1 at. %, the films grown at the lowest temperatures making an exception with about 0.4 at. % of hydrogen.

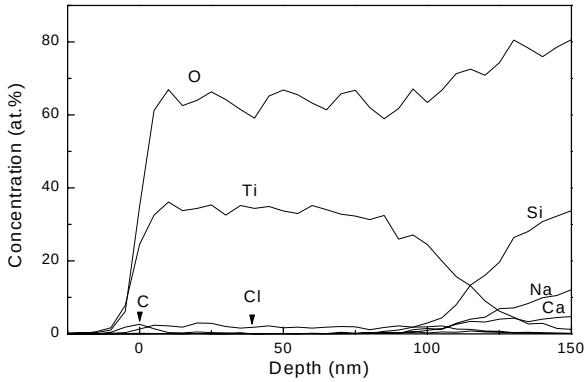

Figure 17. Element depth profiles of a TiO_2 film deposited at 150 °C as analysed by TOF-ERDA.

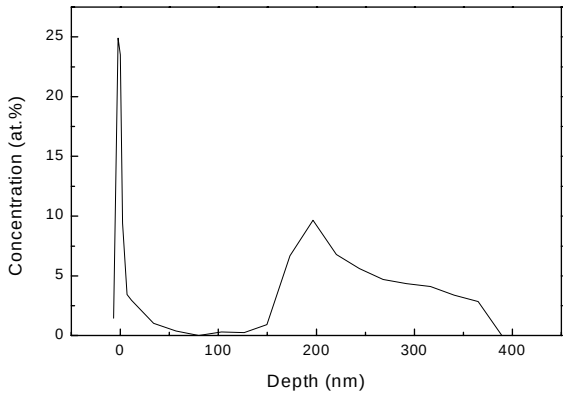

Figure 18. Hydrogen depth profiles in a TiO_2 film deposited at 250 °C as analysed by NRB.

The refractive indices measured at λ=580 nm increase from 2.41 to 2.58 with increasing growth temperature from 150 to 400 °C. A high refractive index indicates dense film structure and is combined to low hydrogen content.[149] Thus, the film quality improves when the growth temperature is increased. The crystallinity of the films, however, introduces grain boundaries that lower the film density and may serve as weak points in corrosion protection. Because of the grain boundaries TiO_2 films alone are not necessarily good protective coatings even though the chemical stability of the films is good: the films on glass could be etched only with 80 % H_2SO_4 at 110 °C with a rate of about 2 nm/h (films deposited at 250 – 400 °C), 7 nm/h (film deposited at 200 °C) and 6 nm/min (film deposited at 150 °C).

4.2.2. Corrosion Protection Properties

The corrosion protection properties of the Al_2O_3 and TiO_2 films on stainless steel substrates were investigated by electrochemical impedance spectroscopy (EIS). The work was carried out in the Laboratory of Corrosion and Materials Chemistry at the Helsinki University of Technology. The experimental details and a more detailed analysis of the corrosion protection properties are presented in paper II.

Al_2O_3: At first the films seemed to resist the 3.5 wt.% NaCl solution, but after a few weeks the electrolyte had penetrated some weak points of the coating. The films

grown at 250 °C appeared to be the best. The films were thought to dissolve slowly due to their amphoteric nature. This dissolution was observed also visually as the reflection colour of the films changed during immersion.

TiO_2: The optimum deposition temperature seemed to be 200 – 300 °C. The films grown at 300 °C resisted the NaCl electrolyte better than those deposited at lower temperatures. The crystalline nature of the films enabled the electrolyte to penetrate the coating through grain boundaries and cause corrosion of the underlying substrate. This phenomenon was best seen in the case of the films grown at 400 °C.

TiO_2 films were tested also in an acidic environment in 1 mol/l HCl. Again due to the grain boundaries or pores, the corrosive media was able to penetrate through the coating and cause corrosion of the steel substrate.

Al_2O_3–TiO_2 multilayer structures were prepared to combine the good characteristics of both film materials, i.e., the grain boundary free, dense structure of Al_2O_3 and the inherent chemical stability of TiO_2. The intermediate amorphous Al_2O_3 layers prevent the grain boundaries in crystalline TiO_2 from extending through the whole structure (Fig. 19). Four different kinds of multilayers were made: 2x(Al_2O_3-TiO_2), 4x(Al_2O_3-TiO_2), 8x(Al_2O_3-TiO_2) and 20x(Al_2O_3-TiO_2). These films were grown at 250 ºC and the total thickness of the films was about 400 nm.

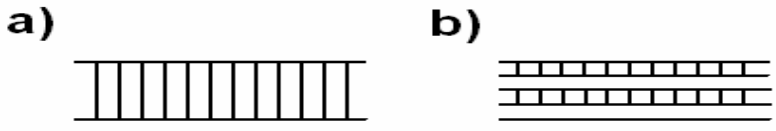

Figure 19. a) A single TiO_2 layer. b) An Al_2O_3-TiO_2 multilayer structure.

No clear tendency was observed between the corrosion protection properties and the number of layer pairs in the coating with a total thickness of 400 nm. The best of the coatings studied seemed to be the one with 20 Al_2O_3–TiO_2 double layers. No clear visual changes or corrosion were observed in any of the multilayer coatings after 12 weeks immersion in 3.5 wt.% NaCl. The multilayer coating clearly offered better protection against corrosion compared to the single layer oxides.

4.2.3 Reaction Mechanism Studies on the Me_2AlCl – D_2O ALD Process [III]

The reaction mechanism studies on the Me_2AlCl – D_2O process are the first where there are two different kinds of ligands attached to the metal. The motivation of this study was to investigate whether the methyl groups or the chloride ion preferentially interacts with the –OD groups during adsorption.

Reaction mechanism The film growth proceeds via surface reactions, in which ligands are exchanged with hydroxyl groups. Suggestions for these exchange reactions are presented in Appendix A, it is possible that these reactions occur simultaneously. There are two apparent reaction by-products: DCl and CH_3D, molecular ions of which are detected at *m/z*=37 and *m/z*=17, respectively.

The QMS data suggests that a large part of the methyl ligands is released during the Me_2AlCl pulse and most of the chloride ligands during the water pulse. An *n* value referring to the number of ligands released per one Al during the Me_2AlCl pulse can be calculated separately for both ligands. These values are referred to as n_{Me} and n_{Cl} and are obtained as follows: the amount of the given by-product detected during the Me_2AlCl pulse is divided by its total amount, i.e. the amount detected during both precursor pulses altogether. As there are two –Me ligands and one –Cl ligand in Me_2AlCl, the values of n_{Me} and n_{Cl} can be in the ranges of 0 – 2 and 0 – 1, respectively. These separate values are then added together to give the total number of ligands (n_{Me} + n_{Cl}) reacting during the metal precursor pulse. This reaction can be depicted by Reaction 17:

$(n_{Me}+n_{Cl})$ –OD (s) + $Me_2AlCl \rightarrow$

$$(–O–)_{(nMe+nCl)}AlMe_{(2-nMe)}Cl_{(1-nCl)}\ (s) + n_{Me}\ CH_3D\ (g) + n_{Cl}\ DCl\ (g) \quad (17)$$

The total *n* value decreases from 1.66 to 0.97 while the temperature increases from 150 to 400 ºC, so more than half of the ligands are released during the Me_2AlCl pulse at the lowest temperature and less than one ligand at the highest.

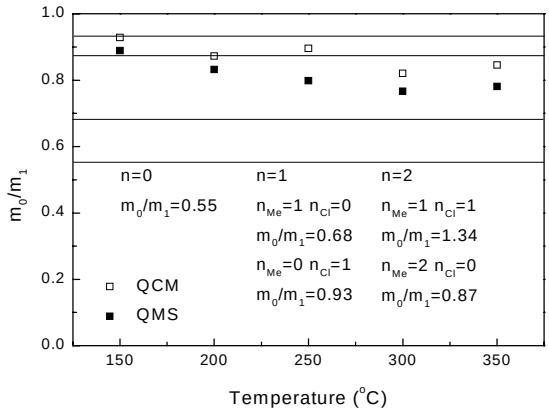

Figure 20. m_0/m_1 obtained from the QCM data at different temperatures (open squares) and calculated using the *n* values from the QMS data (solid squares). These values refer to possible reactions presented in Appendix A. *n* refers to the total number of ligands released during the Me_2AlCl pulse. It can be divided into n_{Me} and n_{Cl} (see Equation 17), which refer to the number of –Me and –Cl ligands, respectively, released during the Me_2AlCl pulse per one Al.

The QMS results indicate that more than one of the reactions presented in Appendix A take place at the same time. Therefore, evaluation of the reaction mechanism from the QCM data is complicated. Usually the measured m_0/m_1 value is compared with theoretical values (Appendix A). In this case, it can be done only under the assumption that a single reaction takes place at a time. So the following interpretation of the QCM data should be regarded only suggestive.

The m_0/m_1 values calculated from the QCM data suggest (Fig. 20) that e.g. at 150 ºC the chloride ligand leaves already during the Me_2AlCl pulse and the methyls during the water pulse. The values measured for temperatures above 200 ºC suggest a

mechanism where the methyls would be released during the Me_2AlCl pulse and the chloride during the water pulse, which is in accordance with QMS. m_0/m_1 values can also be calculated using the n_{Me} and n_{Cl} values obtained from the QMS data (Fig. 20). As m_1 is the change in mass during the Me_2AlCl adsorption, it equals to the change in surface species in Reaction 17 and it can be calculated as follows: m_1 = M(Al) + (2-n_{Me})M(Me) + (1-n_{Cl})M(Cl) - (n_{Me}+n_{Cl})M(D). m_0 refers to the Al_2O_3 deposited, in this case, when only one Al is involved, M($AlO_{1.5}$). The calculated values are reasonably close to those measured with the QCM. There is some difference between the measured and calculated value at 250 °C, but both values still refer to a similar reaction mechanism. At 150 °C, there is a contradiction in the values. Although they are very close to each other, they refer to different mechanisms if they are interpreted by a single reaction (Appendix A). As it obvious that more than one reaction is applied simultaneously, QMS more reliably gives the average reaction mechanism.

Growth Rate The growth rate according to QMS and QCM is depicted in Fig. 21. Optically determined growth rate from an earlier film deposition study is included for comparison. [28] The growth rate obtained from the QMS data is the total amount of *m/z*=17 and *m/z*=37 released during both precursor pulses. The data is normalised to unity at 250 ºC. The results are in good accordance with each other. At 150 ºC the value obtained from QMS measurements is low compared to the QCM and ALD results. It has been shown that the films deposited below 200 ºC contain relatively high amounts of hydrogen, chlorine and carbon impurities.[28] These impurities are incorporated into the film during the film growth by incomplete surface reactions, i.e. the ligands are not removed completely. The QMS measures gaseous products originating from the surface reactions, and when these reactions are not complete, the amount of by-products is lower than would be expected based on the growth rate. Hence, the low growth rate compared to QCM and optically determined (taken from Ref. 28). Above 250 ºC the growth rate decreases slowly, which is usually attributed to the decreasing hydroxyl group density on the surface.

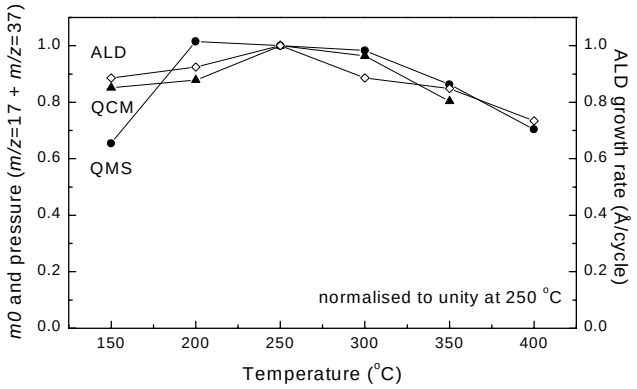

Figure 21. The growth rate in the Me_2AlCl–D_2O process measured with QMS and QCM. Optically determined growth rate[28] for the Me_2AlCl–H_2O ALD process is included for comparison.

4.2.4 Reaction Mechanism Studies on the $TiCl_4$ – D_2O ALD Process [IV]

Reaction mechanism The ALD growth of TiO_2 from $TiCl_4$ and water has been suggested to proceed via ligand exchange reactions taking place on the surface. In these reactions the incoming $TiCl_4$ reacts with the surface hydroxyl groups releasing hydrogen chloride. The subsequent water pulse then releases the possibly remaining –Cl ligands restoring the hydroxyl covered starting surface. Suggested reaction mechanisms are presented in Appendix B.

The only reaction by-product that was observed was DCl, which was produced during both the $TiCl_4$ and D_2O pulses. An *n* value referring to the number of –Cl ligands released during the $TiCl_4$ pulse (Appendix B) can be calculated from the QMS results, i.e. from the amounts of DCl released. These values (Fig. 22) show that the number of released –Cl ligands decreases with increasing temperature and ,hence, the number of –OD groups also decreases. At 150 ºC the incoming $TiCl_4$ interacts with about 2 –OD groups and with less than one at 400 ºC, which means that at the higher temperatures the growth must at least partially proceed via dissociative chemisorption on dehydroxylated surface:

$$Ti(–O–)_2Ti\ (s) + TiCl_4\ (g) \rightarrow Ti(Cl)–O–Ti(OTiCl_3)\ (s) \qquad (18)$$

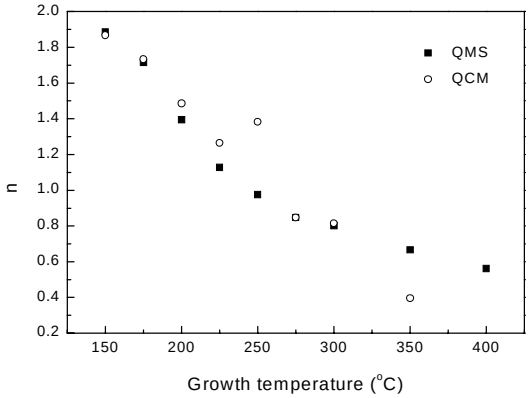

Figure 22. *n* values in $TiCl_4$ – D_2O process as calculated from the QCM and QMS data for the reaction $TiCl_4$ + D_2O.

Other volatile by-products have been suggested in the literature[31,142,150], e.g. Cl_2, $Ti(OD)_xCl_y$ and TiO_xCl_y. None of those were observed in this study by QMS. Either they were not formed, their lifetime was too short or the amount was too small to be detected.

Growth rate The growth rate can be depicted by the total amount of DCl released during one ALD cycle as measured by QMS. The m_0 obtained from the QCM results also refers to the film growth rate. Both of these are shown in Figure 23, the results are normalised to unity at 250 ºC.

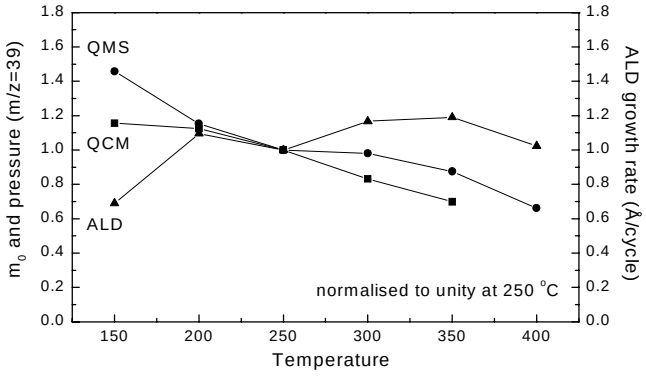

Figure 23. The normalised weight change during one complete ALD cycle (m_0, labelled QCM) and the total amount of reaction by-products (DCl, *m/z*=39, labelled QMS) as a function of reaction temperature. The growth rates measured optically taken from paper II (labelled ALD) are included for comparison.

Below 200 ºC the growth rate deduced from the QMS results is much higher than that of QCM. This comes from the high DCl amounts released during the $TiCl_4$ pulse. It could be explained by adsorption of molecular water onto the substrates and the walls of the reaction chamber, and its subsequent reaction with the $TiCl_4$ pulse. Between 200 and 250 ºC the results seem to be in good accordance with each other. The QMS and QCM results are still in rather good agreement above 250 ºC: the growth rate decreases steadily as the temperature increases. The difference between the growth rates obtained in the *in situ* studies and the optically determined ones from the conventional ALD process might be caused by different reactor design and process conditions (e.g. carrier gas flow rate).

4.3 ZrO_2 [V,VI]

As already was presented in Tables 1 and 4, a number of precursors have been investigated for the ALD of ZrO_2. The halides are high melting point solid sources with a very fine particle size, which leads to a risk of particle transport to the substrate and into the films. The β-diketonates and cyclopentadienyls have been used with ozone as the oxygen source. Ozone causes oxidation of silicon, so these processes are unlikely to be suitable for applications in silicon technology. $Zr(O^tBu)_4$ has been observed to decompose extensively, which for example leads to hydrogen and carbon residues in the films. It could be possible to stabilise the alkoxide by adding a donor-functionalised ligand, dmae (dmae = $[OCH_2CH_2N(CH_3)_2]$). The ALD deposition of ZrO_2 from $Zr(dmae)_4$, $Zr(dmae)_2(O^tBu)_2$, $Zr(dmae)_2(O^iPr)_2$ and H_2O is briefly presented and discussed in this chapter. The results obtained from the film growth experiments and the *in situ* studies are reviewed together from the film growth point of view. The reaction mechanism is discussed separately in the end of the chapter.

Pulse length. No saturation of the growth rate was observed with any of the precursors studied when the Zr precursor pulse was varied from 0.2 to 1.5 s. As no tendency toward saturation was observed, the pulse length was not elongated over 1.5 s. The non-saturative growth was attributed to decomposition of the metal precursor. The growth rate settled to a different level depending on the precursor being 0.50 – 1.08 Å/cycle for $Zr(dmae)_4$, 0.58 – 1.32 Å/cycle for $Zr(dmae)_2(O^tBu)_2$ and 0.70 – 1.48

Å/cycle for $Zr(dmae)_2(O^iPr)_2$. The H_2O pulse length did not have a significant effect on the growth rate.

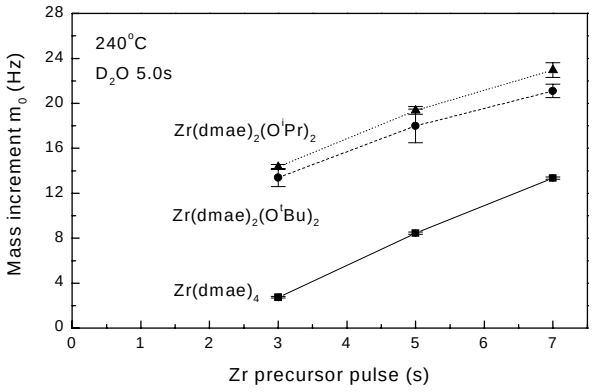

Figure 24. The mass increment detected with the QCM at various Zr precursor pulse lengths at 240 °C.

The nonsaturative growth can more clearly be seen in the QCM data presented in Figures 24 and 25 where the mass increment during one ALD cycle (m_0) is presented. The m_0 increases steadily as the Zr precursor pulse is elongated from 3.0 to 7.0 s with all three precursors. In Figure 25 the $Zr(dmae)_4$ pulse length has been varied from 1.0 to 30.0 s. These results support the assumption of precursor decomposition. Variation of the H_2O pulse length from 0.2 to 1.5 s did not have such an effect on m_0, thus indicating that either the growth settled to a certain level or lower m_0 values were obtained with the longer H_2O pulses.

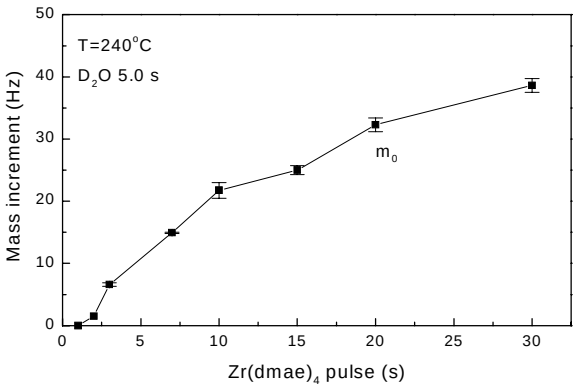

Figure 25. The effect of elongated $Zr(dmae)_4$ pulse on m_0 at 240 °C.

During the TOF-ERDA analysis, impurities were found to escape from the films. This is apparently due to the impurity species decomposing effect of heavy ion beam. For that reason, the TOF-ERDA results are not very accurate, but some conclusions can be drawn. Elongating the Zr precursor pulse from 0.2 to 1.5 s at 240 °C did not significantly increase the impurity content. There was at least 30 at.% of hydrogen in the film grown from $Zr(dmae)_4$, and the same amount was detected when the longer Zr precursor pulse had been applied. For $Zr(dmae)_2(O^tBu)_2$ the hydrogen content was at least 11 at.%. In the case of $Zr(dmae)_2(O^iPr)_2$ no accurate values could be determined for the film grown using 0.2-s Zr precursor pulse, but the film contained substantial amounts of hydrogen. The carbon and nitrogen contents were also about the same with both pulse lengths, for example, at least 10 at.% of carbon and 1 at.% of nitrogen in the films grown from $Zr(dmae)_4$.

There is a contradiction between the impurity contents and refractive indices in the case of elongated Zr precursor pulse. The pulse elongation from 0.2 to 1.5 s does not affect the impurity contents, but it affects the refractive index: 1.92 → 1.79 for $Zr(dmae)_4$, 1.87 → 1.82 for $Zr(dmae)_2(O^tBu)_2$ and 1.89 → 1.83 for $Zr(dmae)_2(O^iPr)_2$. A lower refractive index would suggest a higher hydrogen content.[149] One should keep in mind, though, that this time the TOF-ERDA results are only qualitative, the real amounts might be completely different.

Decomposition The assumed decomposition of the precursor was tested by pulsing only the Zr precursor on glass and ZrO_2 film. In the film growth experiments no or barely any film was obtained at 240 °C with a short 0.2-s Zr precursor pulse. A longer pulse length (1.5 s) and a higher deposition temperature (340 °C) was tested with $Zr(dmae)_2(O^iPr)_2$, but no film was deposited. These results suggest that the decomposition may be induced by the surface OH groups that are formed in exchange reactions with water.

A reaction mechanism for heterogeneous decomposition of $Zr(O^tBu)_4$ has been suggested by Cameron and George[151]. First $Zr(O^tBu)_4$ reacts with a surface hydroxyl group and becomes bound to the surface. In this reaction a t-butoxide ligand is eliminated as t-butanol (Reaction 19).

$$–(OH)\ (s) + Zr(O^tBu)_4 \rightarrow –O–\ Zr(O^tBu)_3\ (s) + {}^tBuOH \qquad (19)$$

Second, the remaining $–O^tBu$ groups may decompose by β-hydride elimination producing isobutylene and creating new OH groups on the surface (Reaction 20).

$$Zr–(O^tBu)\ (s) \rightarrow Zr–(OH)\ (s) + CH_2C(CH_3)_2 \qquad (20)$$

The occurrence of these reactions is supported by the QCM data. When only $Zr(dmae)_2(O^tBu)_2$ was pulsed, a significant mass increment (m_0) was observed during the first couple of pulses (Fig. 26). At this stage, the surface OH groups are most probably slowly consumed according to Reaction 19. After these first pulses, m_0 settles to a certain level, suggesting that the ligands decompose by creating new surface sites according to reaction 20. The number of these OH sites formed by β-elimination is low compared to the initial OH coverage, hence the mass increment is much smaller. Without decomposition no mass uptake should take place at all when only one precursor is pulsed.

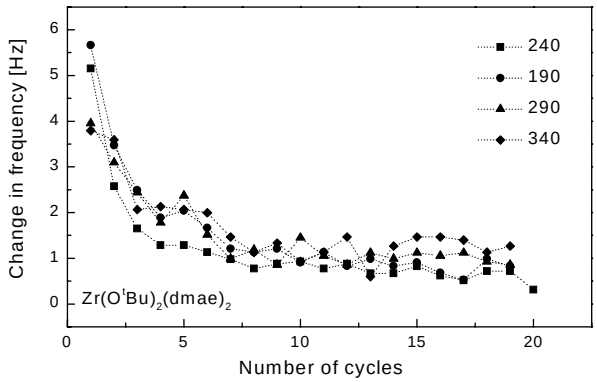

Figure 26. The m_0 obtained from the QCM data measured during 20 $Zr(dmae)_2(O^tBu)_2$ pulses at various temperatures.

The QMS results may also support reaction 20 as m/z=56 which refers to $[CH_2C(CH_3)_2]^+$ was detected. The alcohol formed in Reaction 19 was not observed, though. It is possible that it was not formed, the amounts were too small to be

detected or it fragmented in the ion source. When only $Zr(dmae)_4$ or $Zr(dmae)_2(O^iPr)_2$ was pulsed, results similar to $Zr(dmae)_2(O^tBu)_2$ were obtained with the QCM.

Temperature. The deposition temperature was varied between 190 and 340 °C. As the precursors were evaporated at 150 and 170 °C, 190 °C was chosen for the lowest deposition temperature. Due to the decomposition tendency of the precursors, 340 °C was not exceeded. The deposition temperature did not have a large effect on the growth rate. It increased slightly at higher temperatures in the case of $Zr(dmae)_4$ and $Zr(dmae)_2(O^tBu)_2$ which could be attributed to precursor decomposition. In the case of $Zr(dmae)_2(O^iPr)_2$ the growth rate decreased slightly with increasing temperature. Surprisingly, barely any film was deposited at 190 °C with $Zr(dmae)_4$, probably due to very slow surface reactions.

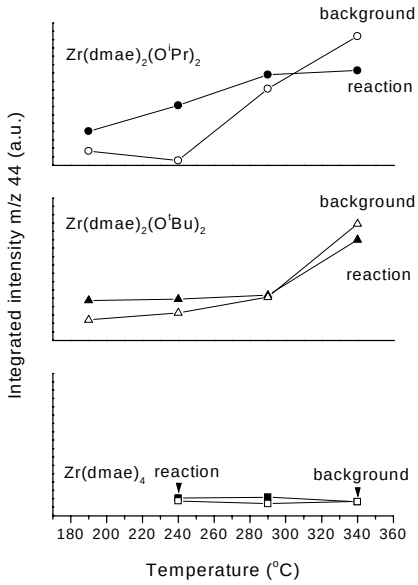

Figure 27. The amount of *m/z*=44 measured by QMS at 240 °C (reaction = the amount detected during ALD reaction, background = the amount coming from the Zr precursor).

The suggested decomposition at the higher temperatures is supported by the QMS measurements, but surprisingly though, there is some contradiction. In Figure 27 can be seen that the background signals coming from the Zr precursors are dependent on

temperature in the case of $Zr(dmae)_2(O^tBu)_2$ and $Zr(dmae)_2(O^iPr)_2$, but there seems to be no such a dependence in the case of $Zr(dmae)_4$. At 340 °C the background signal exceeds the amount of the same mass detected during ALD reactions.

The refractive index increased with increasing temperature indicating a more dense film structure. Higher refractive index suggests also less impurities in the film. This suggestion is supported by the TOF-ERDA results on films deposited at 240 and 340 °C. Impurities were removed from the films deposited at 240 °C during analysis but in the case of the films deposited at 340 °C this did not occur. The films contained about 13 at.% of hydrogen and about 5 at.% carbon. These amounts are about half of those measured for films grown at 240 °C.

Thermal annealing at 500 °C under N_2 had a noticeable effect on the refractive index and film thickness. The refractive index was improved from 1.82 to 1.99, from 1.91 to 2.08 and from 1.88 to 2.06 for $Zr(dmae)_4$, $Zr(dmae)_2(O^tBu)_2$ and $Zr(dmae)_2(O^iPr)_2$, respectively. A 30 - 40 % thickness decrease was observed in the films deposited at 240 °C during annealing which together with the increased refractive index indicates densification of the film material.

Crystallinity of the as-deposited films varied according to the deposition temperature: the films grown at 190 - 240 °C were amorphous and the films grown at 290 - 340 °C were nanocrystalline. The annealing turned also the amorphous films into crystalline. The XRD results are presented in more detail in paper VI.

Reaction mechanism As all three precursors decompose at the higher temperatures and as we were not able to find an ion coming exclusively from one of the ligands, it was not possible to deduce any detailed reaction mechanism from the QMS and QCM data. Appendeces C, D and E suggest possible reaction mechanisms occurring in an ideal case when the film growth proceeds only via ligand exchange reactions on the film surface.

During the $Zr(dmae)_4$ pulse the precursor should react with the surface hydroxyl groups releasing dmae ligands as deuterated dimethylaminoethanol, dmaeD (Reaction

21 below). The remaining ligands should then react with the incoming water and the surface should again become hydroxyl covered (Reaction 22 below).

$$2\ \text{–OD (s)} + \text{Zr(dmae)}_4\ \text{(g)} \rightarrow (\text{–O–})_2\text{Zr(dmae)}_2\ \text{(s)} + 2\ \text{dmaeD (g)} \qquad (21)$$

$$(\text{–O–})_2\text{Zr(dmae)}_2\ \text{(s)} + 2\ \text{D}_2\text{O (g)} \rightarrow (\text{–O–})_2\text{Zr(OD)}_2\ \text{(s)} + 2\ \text{dmaeD (g)} \qquad (22)$$

The main reaction by-product dmaeD should be observed by QMS as *m/z*=90, $[\text{dmaeD}]^+$. However, hardly any of this mass was observed which suggests that it either did not form or it was fragmented, the latter one being the most probable explanation. Fragmentation is supported also by the fact that significant amounts of the main fragment coming from α-cleavage, *m/z*=58 $[\text{CH}_2\text{N(CH}_3)_2]^+$, was detected. Another fragment produced by a secondary rearrangement reaction, *m/z*=44 $[\text{CH}_2\text{NHCH}_3]^+$, was also detected in high amounts. These ions were detected during both the Zr precursor pulse and the water pulse.

In the case of $\text{Zr(dmae)}_2(\text{O}^t\text{Bu})_2$, the situation is more complicated as there are two different ligands attached to the metal. Releasing these ligands produces two possible reaction by-products or a combination of those (Reactions 23 – 28 below).

$$2\ \text{–OD (s)} + \text{Zr(dmae)}_2(\text{O}^t\text{Bu})_2\ \text{(g)} \rightarrow (\text{–O–})_2\text{Zr(dmae)}_2\ \text{(s)} + 2\ ^t\text{BuOD (g)} \qquad (23)$$

$$(\text{–O–})_2\text{Zr(dmae)}_2\ \text{(s)} + 2\ \text{D}_2\text{O (g)} \rightarrow (\text{–O–})_2\text{Zr(OD)}_2\ \text{(s)} + 2\ \text{dmaeD (g)} \qquad (24)$$

$$2\ \text{–OD (s)} + \text{Zr(dmae)}_2(\text{O}^t\text{Bu})_2\ \text{(g)} \rightarrow (\text{–O–})_2\text{Zr}(\text{O}^t\text{Bu})_2\ \text{(s)} + 2\ \text{dmaeD (g)} \qquad (25)$$

$$(\text{–O–})_2\text{Zr}(\text{O}^t\text{Bu})_2\ \text{(s)} + 2\ \text{D}_2\text{O (g)} \rightarrow (\text{–O–})_2\text{Zr(OD)}_2\ \text{(s)} + 2\ ^t\text{BuOD (g)} \qquad (26)$$

$$2\ \text{–OD (s)} + \text{Zr(dmae)}_2(\text{O}^t\text{Bu})_2\ \text{(g)} \rightarrow (\text{–O–})_2\text{Zr(dmae)}(\text{O}^t\text{Bu})\ \text{(s)} + \text{dmaeD (g)} + ^t\text{BuOD (g)} \qquad (27)$$

$$(\text{–O–})_2\text{Zr(dmae)}(\text{O}^t\text{Bu})\ \text{(s)} + 2\ \text{D}_2\text{O (g)} \rightarrow (\text{–O–})_2\text{Zr(OD)}_2\ \text{(s)} + \text{dmaeD (g)} + ^t\text{BuOD} \qquad (28)$$

The main reaction by-products should be dmaeD (*m/z*=90) and ^{t}BuOD (*m/z*=75), neither of which were observed. Again, fragments at *m/z*=58 $[CH_2N(CH_3)_2]^+$ and *m/z*=60 $[(CH_3)_2COD]^+$ were detected.

$Zr(dmae)_2(O^iPr)_2$ should react in a similar manner as $Zr(dmae)_2(O^tBu)_2$: either both dmae or both O^iPr ligands are released at the same time or one dmae and one O^iPr ligand is released. The main reaction by-products should be dmaeD (*m/z*=90, not detected) and Pr^iOD (*m/z*=61), which again was observed as a fragment: $[CH_3CHOD]^+$ (*m/z*=46).

5. Concluding Remarks

The effect of water dose on the growth rate of ALD deposited Al_2O_3 was examined in detail using Me_3Al and H_2O as precursors. The growth rate could be enhanced by increasing the water dose, which is believed to be due to increased density of hydroxyl groups on the film surface after the water pulse. The increased OH density can be caused by more effective removal of CH_3 ligands or saturation of coordinatively unsaturated surface oxygen and aluminium. The increase of water dose did not affect the film quality.

A number of other ALD oxide processes were also examined. In most of them, the growth rate could be increased by increasing the water dose while the film properties remained unaffected, and sometimes the film purity was even improved.

The suitability of ALD grown Al_2O_3 and TiO_2 for corrosion protection coatings was studied. The amphoteric nature of Al_2O_3 makes it nonresistant against acidic and basic solutions. The films were immersed in NaCl solution and already after a few weeks the solution had penetrated through some weak points in the coating. In the case of TiO_2, the material itself was more resistant, but due to its crystallinity the corrosive media was able to reach the substrate, most likely through grain boundaries. The combination of alternating Al_2O_3 and TiO_2 layers appeared to resist corrosive media.

The growth of Al_2O_3 from dimethylaluminium chloride and water was examined in situ. The QMS results indicated that –Me and –Cl ligands are released during both

precursor pulses. It is evident that the growth proceeds via more than one of the suggested reactions occurring simultaneously.

The ALD process $TiCl_4$ – D_2O appeared to take place via –OD to –O–$TiCl_x$ and –Cl to –OD surface exchange reactions, as had been suggested earlier. The number of –OD groups reacting during the $TiCl_4$ pulse decreased with increasing deposition temperature, which indicates that the surface dehydroxylates at elevated temperatures. Other volatile reaction by-products apart from DCl, for example TiO_xCl_y, were not observed with QMS, which means they were not formed or the amount was too small, or their lifetime was too short to be detected.

ZrO_2 films were deposited from H_2O and new aminoalkoxide Zr precursors, $Zr(dmae)_4$, $Zr(dmae)_2(O^tBu)_2$, $Zr(dmae)_2(O^iPr)_2$. The processes were not pure ALD as no saturation of the surface was achieved due to decomposition of the aminoalkoxide compounds. Most likely for the same reason the obtained films contained significant amounts of residual hydrogen and carbon. The decomposition was seen clearly in the QCM results at high temperatures and with long Zr precursor pulses.

References

1. Suntola, T. *Mater. Sci. Rep.* 4 **1989** 261.
2. Suntola, T. *Thin Solid Films* 216 **1992** 84.
3. Ritala, M., Leskelä, M. in *Handbook of Thin Film Materials*, Vol 1, Nalwa, H.S. (Ed.), Academic Press, San Diego **2001**, 103.
4. Leskelä, M., Ritala, M. *Thin Solid Films* 409 **2002** 138.
5. Suntola, T., Antson, J., Pakkala, A., Lindfors, S. *SID 80 Digest* 11 **1980** 108.
6. Ritala, M., Leskelä, M. *Nanotechnol.* 10 **1999** 19.
7. Niinistö, L., Päiväsaari, J., Niinistö, J., Putkonen, M., Nieminen, M. *Phys. Stat. Sol. A* 201 **2004** 1443.
8. Haukka, S., Lakomaa, E.-L., Suntola, T. *Stud. Surf. Sci. Catal.* 120 **1999** 715.
9. Leskelä, M., Ritala, M. *Angew. Chem. Int. Ed.* 42 **2003** 5548.
10. Oya, G., Yoshida, M., Sawada, Y. *Appl. Phys. Lett.* 51 **1987** 1143.
11. Oya, G., Sawada, Y. *J. Cryst. Growth* 99 **1990** 572.
12. Aarik, J., Aidla, A., Jaek, A., Kiisler, A.-A., Tammer, A.-A. *Acta Polytechnol. Scand., Ser. Chem. Technol. Metall.* 195 **1990** 201.
13. Hiltunen, L., Kattelus, H., Leskelä, M., Mäkelä, M., Niinistö, L., Nykänen, E., Soininen, P., Tiitta, M. *Mater. Chem. Phys.* 28 **1991** 379.
14. Ritala, M., Saloniemi, H., Leskelä, M., Prohaska, T., Friedbacher, G., Grassenbauer, M. *Thin Solid Films* 286 **1996** 54.
15. Leskelä, M., Niinistö, L., Nykänen, E., Soininen, P., Tiitta, M. *Acta Polytechnol. Scand., Ser. Chem. Technol. Metall.* 195 **1990** 193.
16. Ritala, M., Kukli, K., Rahtu, A., Räisänen, P.I., Leskelä, M., Sajavaara, T., Keinonen, J. *Science* 288 **2000** 319.
17. Higashi, G.S., Fleming, C.G. *Appl. Phys. Lett.* 55 **1989** 1963.
18. Ott, A.W., McCarley, K.C., Klaus, J.W., Way, J.D., George, S.M. *Appl. Surf. Sci.* 107 **1996** 128.
19. Yun, S.J., Lee, K-H., Skarp, J., Kim, H.R., Nam, K-S. *J. Vac. Sci. Technol. A* 15 **1997** 2993.
20. Ericsson, P., Bengtsson, S., Skarp, J. *Microelectron. Eng.* 36 **1997** 91.
21. Fan, J-F., Sugioka, K., Toyoda, K. *Jpn J. Appl. Phys.* 30 **1991** L1139.
22. Fan, J-F., Toyoda, K. *Appl. Surf. Sci.* 60/61 **1992** 765.
23. Fan, J-F., Toyoda, K. *Jpn J. Appl. Phys.* 32 **1993** L1349.

24. Kumagai, H., Toyoda, K. *Appl. Surf. Sci.* 82/83 **1994** 481.
25. Kumagai, H., Toyoda, K., Matsumoto, M., Obara, M. *Jpn J. Appl. Phys.* 32 **1993** 6137.
26. Kim, J., Chakrabarti, K., Lee, J., Oh, K.-Y., Lee, C. *Mat. Chem. Phys*. 78 **2003** 733.
27. Jeon, W.-S., Yang, S., Lee, C.-S., Kang, S.-W. *J. Electrochem. Soc.* 149 **2002** C306.
28. Kukli, K., Ritala, M., Leskelä, M. Jokinen, J. *J. Vac. Sci. Technol. A* 15 **1997** 2214.
29. Cho, W., Sung, K., An, K.-S., Lee, S.S., Chung, T.-M., Kim, Y. *J. Vac. Sci. Technol. A* 21 **2003** 1366.
30. Desu, S.B. *Mater. Sci. Eng. B* 13 **1992** 299.
31. Ritala, M., Leskelä, M., Nykänen, E., Soininen, P., Niinistö, L. *Thin Solid Films* 225 **1993** 288.
32. Kumagai, H., Matsumoto, M., Kawamura, Y., Toyoda, K., Obara, M *Jpn J. Appl. Phys.* 33 **1994** 7086.
33. Kumagai, H., Matsumoto, M., Toyoda, K., Obara, M., Suzuki, M. *Thin Solid Films* 263 **1995** 47.
34. Kukli, K., Ritala, M., Schuisky, M., Leskelä, M., Sajavaara, T., Keinonen, J., Uustare, T., Hårsta, A. *Chem. Vap. Deposition* 6 **2000** 303.
35. Schuisky, M., Hårsta, A., Aidla, A., Kukli, K., Kiisler, A.-A., Aarik, J. *J. Electrochem. Soc.* 147 **2000** 3319.
36. Schuisky, M., Aarik, J., Kukli, K., Aidla, A., Hårsta, A. *Langmuir* 17 **2001** 5508.
37. Schuisky, M., Kukli, K., Aarik, J., Lu, J., Hårsta, A. *J. Cryst. Growth* 235 **2002** 293.
38. Pore, V., Rahtu, A., Leskelä, M., Ritala, M. *Chem. Vap. Deposition* 10 **2004** 143.
39. Döring, H., Hashimoto, K., Fujoshima, A. *Ber. Bunsenges. Phys. Chem.* 96 **1992** 620.
40. Ritala, M., Leskelä, M., Niinistö, L, Haussalo, P. *Chem. Mater.* 5 **1993** 1174.
41. Ritala, M., Leskelä, M., Rauhala, E. *Chem. Mater.* 6 **1994** 556.
42. Ritala, M., Leskelä, M. *Appl. Surf. Sci.* 75 **1994** 333.

43. Aarik, J., Aidla, A., Mändar, H., Uustare, T., Sammelselg, V. *Thin Solid Films* 408 **2002** 97.
44. Kukli, K., Forsgren, K., Aarik, J., Uustare, T., Aidla, A., Niskanen, A., Ritala, M., Leskelä, M., Hårsta, A. *J. Cryst. Growth* 231 **2001** 262.
45. Kukli, K., Ritala, M., Leskelä, M. *Chem. Vap. Deposition* 6 **2000** 297.
46. Chang, J.P., Lin, Y.-S. *J. Appl. Phys.* 90 **2001** 2964.
47. Putkonen, M., Niinistö, L. *J. Mater. Chem.* 11 **2001** 3141.
48. Putkonen, M., Niinistö, J., Kukli, K., Sajavaara, T., Karppinen, M., Yamauchi, H., Niinistö, L. *Chem. Vap. Deposition* 9 **2003** 207.
49. Chakraborty, A., Mane, A.U., Shivashankar, S.A., Venkataraman, V. *Mat. Res. Soc. Symp. Proc.* 745 **2003** 143.
50. Hausmann, D.M., Kim, E., Becker, J., Gordon, R.G. *Chem. Mater.* 14 **2002** 4350.
51. Nam, W.-H., Rhee, S.-W. *Chem. Vap. Deposition* 10 **2004** 201.
52. Ritala, M., Leskelä, M., Niinistö, L., Prohaska, T., Friedbacher, G., Grassenbauer, M. *Thin Solid Films* 250 **1994** 72.
53. Kukli, K., Ritala, M., Leskelä, M., Sajavaara, T., Keinonen, J., Jones, A.C., Roberts, J.L. *Chem. Mater.* 15 **2003** 1722.
54. Kukli, K., Ritala, M., Leskelä, M., Sajavaara, T., Keinonen, J., Jones, A.C., Roberts, J.L. *Chem. Vap. Deposition* 9 **2003** 315.
55. Conley, J.F., Ono, Y., Tweet, D.J., Zhuang, W., Solanki, R. *J. Appl. Phys.* 93 **2003** 712.
56. Kukli, K., Ritala, M., Sajavaara, T., Keinonen, J., Leskelä, M. *Chem. Vap. Deposition* 8 **2002** 199.
57. Kukli, K., Ritala, M., Leskelä, M., Sajavaara, T., Keinonen, J., Jones, A.C., Tobin, N.L. *Chem. Vap. Deposition* 10 **2004** 91.
58. Forsgren, K., Hårsta, A., Aarik, J., Aidla, A., Westlinder, J., Olsson, J. *J. Electrochem. Soc.* 149 **2002** F139.
59. Kukli, K., Ritala, M., Sundqvist, J., Aarik, J., Lu, J., Sajavaara, T., Leskelä, M., Hårsta, A. *J. Appl. Phys.* 92 **2002** 5698.
60. Sundqvist, J., Hårsta, A., Aarik, J., Kukli, K., Aidla, A. *Thin Solid Films* 427 **2003** 147.
61. Lin, Y.-S., Puthenkovilakam, R, Chang, J.P. *Appl. Phys. Lett.* 81 **2002** 2041.

62. Chang, H.S., Baek, S.-K., Park, H., Hwang, H., Oh, J.H., Shin, W.S., Yeo, J.H., Hwang, K.H., Nam, S.W., Lee, H.D., Song, C.L., Moon, D.W., Cho, M.-H. *Electrochem. Solid-State Lett.* 7 **2004** F42.
63. Pessa, M., Mäkelä, R., Suntola, T. *Appl. Phys. Lett.* 38 **1981** 131.
64. Kattelus, H., Ylilammi, M., Salmi, J., Ranta-Aho, T., Nykänen, E., Suni, I. *Mater. Res. Soc. Symp. Proc.* 284 **1993** 511.
65. Kukli, K., Aarik, J., Aidla, A., Kohan, O., Uustare, T., Sammelselg, V. *Thin Solid Films* 260 **1995** 135.
66. Kukli, K., Ritala, M., Matero, R., Leskelä, M. *J. Cryst. Growth* 212 **2000** 459.
67. Kukli, K., Ritala, M., Leskelä, M. *Chem. Mater.* 12 **2000** 1914.
68. Kukli, K., Aarik, J., Aidla, A., Forsgren, K., Sundqvist, J., Hårsta, A., Uustare, T., Mändar, H., Kiisler, A.-A. *Chem. Mater.* 13 **2001** 122.
69. Sundqvist, J., Högberg, H., Hårsta, A. *Chem. Vap. Deposition* 9 **2003** 245.
70. Kukli, K., Ritala, M., Leskelä, M. *J. Electrochem. Soc.* 142 **1995** 1670.
71. Hausmann, D.M., de Rouffignac, P., Smith, A., Gordon, R., Monsma, D. *Thin Solid Films* 443 **2003** 1.
72. George, S.M., Sneh, O., Dillon, A.C., Wise, M.L., Ott, A.W., Okada, L.A., Way, J.D. *Appl. Surf. Sci.* 82/83 **1994** 460.
73. Sneh, O., Wise, M.L., Ott, A.W., Okada, L.A., George, S.M. *Surf. Sci.* 334 **1995** 135.
74. Klaus, J.W., Ott, A.W., Johnson, J.M., George, S.M. *Appl. Phys. Lett.* 70 **1997** 1092.
75. Klaus, J.W., Sneh, O., George, S.M. *Science* 278 **1997** 1934.
76. Klaus, J.W., Sneh, O., Ott, A.W., George, S.M. *Surf. Rev. Lett.* 6 **1999** 435.
77. Klaus, J.W., George, S.M. *Surf. Sci.* 447 **2000** 81.
78. Park, J.-E., Ku, J.-H., Lee, J.-W., Yang, J.-H., Chu, K.-S., Lee, S.-H., Park, M.-H., Lee, N.-I., Kang, H.-K., Suh, K.-P. *IEDM Dig.* **2002** 229.
79. Gasser, W., Uchida, Y., Matsumura, M. *Thin Solid Films* 250 **1994** 213.
80. Morishita, S., Gasser, W., Usami, K., Matsumura, M. *J. Non-Cryst. Solids* 187 **1995** 66.
81. Morishita, S., Uchida, Y., Matsumura, M. *Jpn J. Appl. Phys.* 34 **1995** 5738.
82. Seim, H., Mölsä, H., Nieminen, M., Fjellvåg, H., Niinistö, L. *J. Mater. Chem.* 7 **1997** 449.
83. Nieminen, M., Putkonen, M., Niinistö, L. *Appl. Surf. Sci.* 174 **2001** 155.

84. Lim, B.S., Rahtu, A., Gordon, R.G. *Nature Mater.* 2 **2003** 749.
85. Mölsä, H., Niinistö, L., Utriainen, M. *Adv. Mater. Opt. Electron.* 4 **1994** 389.
86. Putkonen, M., Sajavaara, T., Johansson, L.-S., Niinistö, L. *Chem. Vap. Deposition* 7 **2001** 44.
87. Niinistö, J., Putkonen, M., Niinistö, L. *Chem. Mater.* 16 **2004** 2953.
88. Mölsä, H., Niinistö, L. *Mater. Res. Soc. Symp. Proc.* 335 **1994** 341.
89. Päiväsaari, J., Putkonen, M., Niinistö, L. *J. Mater. Chem.* 12 **2002** 1828.
90. Päiväsaari, J., Putkonen, M., Sajavaara, T., Niinistö, L. *J. Alloys Comp.* 374 **2004** 124.
91. Putkonen, M., Nieminen, M., Niinistö, J., Niinistö, L., Sajavaara, T. *Chem. Mater.* 13 **2001** 4701.
92. Kosola, A., Päiväsaari, J., Niinistö, L. to be published in *Thin Solid Films*
93. Scarel, G., Bonera, E., Wiemer, C., Tallarida, G., Spiga, S., Fanciulli, M., Fedushkin, I.L., Schumann, H., Lebedinskii, Yu., Zenkevich, A. *Appl. Phys. Lett.* 85 **2004** 630.
94. Päiväsaari, J., Putkonen, M., Niinistö, L. *Thin Solid Films* 472 **2005** 275.
95. Badot, J.C., Ribes, S., Yousfi, E.B., Vivier, V., Pereira-Ramos, J.P., Baffier, N., Lincot, D. *Electrochem. Solid-State Lett.* 3 **2000** 485.
96. Kukli, K., Ritala, M., Leskelä, M., Lappalainen, R. *Chem. Vap. Deposition* 4 **1998** 29.
97. Hatanpää, T., Ihanus, J., Kansikas, J., Mutikainen, I., Ritala, M., Leskelä, M. *Chem. Mater.* 11 **1999** 1846.
98. Huang, R., Kitai, A.H. *Appl. Phys. Lett.* 61 **1992** 1450.
99. Putkonen, M., Sajavaara, T., Niinistö, L. *J. Mater. Chem.* 10 **2000** 1857.
100. Putkonen, M., Johansson, L.-S., Rauhala, E., Niinistö, L. *J. Mater. Chem.* 9 **1999** 2449.
101. Suntola, T.S., Pakkala, A.J., Lindfors, S.G. *U.S. Patent* 4,389,973, **1983**.
102. Groner, M.D., Fabreguette, F.H., Elam, J.W., George, S.M. *Chem. Mater.* 16 **2004** 639.
103. Skarp, J. *U.S. Patent* 4,486,487, **1984**.
104. Ferrari, S., Dekadjevi, D.T., Spiga, S., Tallarida, G., Wiemer, C., Fanciulli, M. *J. Non-Cryst. Solids* 303 **2002** 29.

105. Zhao, C., Roebben, G., Bender, H., Young, E., Haukka, S., Houssa, M., Naili, M., DeGendt, S., Heyns, M., Van Der Biest, O. *Microelectron. Reliability* 41 **2001** 995.
106. Perkins, C.M., Triplett, B.B., McIntyre, P.C., Saraswat, K.C., Haukka, S., Tuominen, M. *Appl. Phys. Lett.* 78 **2001** 2357.
107. Tsai, W., Carter, R.J., Nohira, H., Caymax, M., Conard, T., Cosnier, V., DeGendt, S., Heyns, M., Petry, J., Richard, O., Vandervorst, W., Young, E., Zhao, C., Maes, J., Tuominen, M:, Schulte, W.H., Garfunkel, E., Gustafsson, T. *Microelectron. Eng.* 65 **2003** 259.
108. Cassir, M., Goubin, F., Bernay, C., Vernoux, P, Lincot, D. *Appl. Surf. Sci.* 193 **2002** 120.
109. Copel, M., Gibelyuk, M., Gusev, E. *Appl. Phys. Lett.* 76 **2000** 436.
110. Ott, A.W., Klaus, J.W., Johnson, J.M., George, S.M., McCarley, K.C., Way, J.D. *Chem. Mater.* 9 **1997** 707.
111. Niilisk, A., Rosental, A., Gerst, A., Sammelselg, V., Uustare, T. *Proc. SPIE* 4318 **2001** 72.
112. Rosental, A., Adamson, P., Gerst, A., Koppel, H., Tarre, A. *Appl. Surf. Sci.* 112 **1997** 82.
113. Rosental, A., Tarre, A., Adamson, P., Gerst, A., Kasikov, A., Niilisk, A. *Appl. Surf. Sci.* 142 **1999** 204.
114. Tarre, A., Rosental, A., Sammelselg, V., Uustare, T. *Appl. Surf. Sci.* 175-176 **2001** 111.
115. Sammelselg, V., Rosental, A., Tarre, A., Niinistö, L., Heiskanen, K., Ilmonen, K., Johansson, L.-S., Uustare, T. *Appl. Surf. Sci.* 134 **1998** 78.
116. Aarik, J., Aidla, A., Kukli, K. *Appl. Surf. Sci.* 75 **1994** 180.
117. Ritala, M., Juppo, M., Kukli, K., Rahtu, A., Leskelä, M. *J. Phys. IV* 9 **1999** Pr8-1021.
118. Juppo, M., Rahtu, A., Ritala, M., Leskelä, M. *Langmuir* 16 **2000** 4034.
119. Rahtu, A., Alaranta, T., Ritala, M. *Langmuir* 17 **2001** 6506.
120. Elam, J.W., Groner, M.D., George, S.M. *Rev. Sci. Instrum.* 73 **2002** 2981.
121. Aarik, J., Aidla, A., Sammelselg, V., Siimon, H., Uustare, T. *J. Cryst. Growth* 169 **1996** 496.
122. Aarik, J., Aidla, A., Mändar, H., Sammelselg, V. *J. Cryst. Growth* 220 **2000** 531.

123. Aarik, J., Aidla, A., Mändar, H., Uustare, T. *Appl. Surf. Sci.* 172 **2001** 148.
124. Kukli, K., Aidla, A., Aarik, J., Schuisky, M., Hårsta, A., Ritala, M., Leskelä, M. *Langmuir* 16 **2000** 8122.
125. Aarik, J., Aidla, A., Uustare, T., Kukli, K., Sammelselg, V., Ritala, M., Leskelä, M. *Appl. Surf. Sci.* 193 **2002** 277.
126. Aarik, J., Aidla, A., Sammelselg, V., Uustare, T., Ritala, M., Leskelä, M. Thin Solid Films 370 **2000** 163.
127. Rahtu, A., Kukli, K., Ritala, M. *Chem. Mater.* 13 **2001** 817.
128. Aarik, J., Aidla, A., Uustare, T., Ritala, M., Leskelä, M. *Appl. Surf. Sci.* 161 **2000** 385.
129. Rahtu, A., Ritala, M. *Chem. Vap. Deposition* 8 **2002** 21.
130. Rahtu, A., Ritala, M. *J. Mater. Chem.* 12 **2002** 1484.
131. Aarik, J., Aidla, A., Kukli, K., Uustare, T. *J. Cryst. Growth* 144 **1994** 116.
132. Siimon, H., Aarik, J. *J. Phys. IV* 5 C5 **1995** 277.
133. Aarik, J., Kukli, K., Aidla, A., Pung, L. *Appl. Surf. Sci.* 103 **1996** 331.
134. Kukli, K., Aarik, J., Aidla, A., Siimon, H., Ritala, M., Leskelä, M. *Appl. Surf. Sci.* 112 **1997** 236.
135. Aarik, J., Aidla, A., Kiisler, A.-A., Uustare, T., Sammelselg, V. *Thin Solid Films* 340 **1999** 110.
136. Forsgren, K., Hårsta, A., Aarik, J., Aidla, A. *Electrochem. Soc. Proc.* 2001-13 **2001** 152.
137. Ylilammi, M., Ranta-Aho, T. *Thin Solid Films* 232 **1993** 56.
138. Jokinen, J., Haussalo, P., Keinonen, J., Ritala, M., Riihelä, D., Leskelä, M. *Thin Solid Films* 289 **1996** 159.
139. Jokinen, J., Keinonen, J., Tikkanen, P., Kuronen, A., Ahlgren, T., Nordlund, K. *Nucl. Instrum. Methods Phys. Rev. B* 119 **1996** 533.
140. Rahtu, A. in "Atomic Layer Deposition of High Permittivity Oxides: Film Growth and *in situ* Studies", Ph.D. thesis, Helsinki **2002**
141. George, S.M., Ott, A.W., Klaus, J.W. *J. Phys. Chem.* 100 **1996** 13121.
142. Haukka, S., Lakomaa, E.-L., Root, A. *J. Phys. Chem.* 97 **1993** 5085.
143. Primet, M., Pichat, P., Mathieu, M.-V. *J. Phys. Chem.* 75 **1971** 1216.
144. Nelson, C.E., Elam, J.W., Cameron, M.A., Tolbert, M.A., George, S.M. *Surf. Sci.* 416 **1998** 341.

145. Kuse, R., Kundu, M., Yasuda, T., Miyata, N., Toriumi, A. *J. Appl. Phys.* 94 **2003** 6411.
146. Lakomaa, E.-L., Root, A., Suntola, T. *Appl. Surf. Sci.* 107 **1996** 107.
147. Dillon, A.C., Ott, A.W., Way, J.D., George, S.M. *Surf. Sci.* 322 **1995** 230.
148. Niinistö, L., Ritala, M., Leskelä, M. *Mater. Sci. Eng. B* 41 **1996** 23.
149. Ottermann, C.R., Bange, K., Wagner, W., Laube, M., Rauch, F. *Surf. Interface Anal.* 19 **1992** 435.
150. Gruy, F., Pijolat, M. *J. Am. Ceram. Soc.* 75 **1992** 663.
151. Cameron, M.A., George, S.M. *Thin Solid Films* 348 **1999** 90.

Appendix A

Reaction mechanism suggestions for Me_2AlCl — D_2O ALD process

n	n_{CH3}	n_{Cl}	**Reactions**	m_0/m_1
0	0	0	$Me_2AlCl\ (g) \rightarrow Me_2AlCl\ (s)$ $Me_2AlCl\ (s) + 1.5\ D_2O\ (g) \rightarrow$ $-AlO_{1.5}\ (s) + 2\ CH_3D\ (g) + DCl\ (g)$	0.55
1	1	0	$-OD\ (s) + Me_2AlCl\ (g) \rightarrow -O-AlMeCl\ (s) + CH_3D\ (g)$ $-O-AlMeCl\ (s) + 1.5\ D_2O\ (g) \rightarrow$ $(-O-)_{1.5}AlOD\ (s) + CH_3D\ (g) + DCl\ (g)$	0.68
1	0	1	$-OD\ (s) + Me_2AlCl\ (g) \rightarrow -O-AlMe_2\ (s) + DCl\ (g)$ $-O-AlMe_2\ (s) + 1.5\ D_2O\ (g) \rightarrow$ $(-O-)_{1.5}AlOD\ (s) + 2\ CH_3D\ (g)$	0.93
2	1	1	$2\ -OD\ (s) + Me_2AlCl\ (g) \rightarrow$ $(-O-)_2AlMe\ (s) + CH_3D\ (g) + DCl\ (g)$ $(-O-)_2AlMe\ (s) + 1.5\ D_2O\ (g) \rightarrow$ $(-O-)_{1.5}Al(OD)_2\ (s) + CH_3D\ (g)$	1.34
2	2	0	$2\ -OD\ (s) + Me_2AlCl\ (g) \rightarrow (-O-)_2AlCl\ (s) + 2\ CH_3D\ (g)$ $(-O-)_2AlCl\ (s) + 1.5\ D_2O\ (g) \rightarrow\ (-O-)_{1.5}Al(OD)_2\ (s) + DCl\ (g)$	0.87
3	2	1	$3\ -OD\ (s) +\ Me_2AlCl\ (g) \rightarrow$ $(-O-)_3Al\ (s) + 2\ CH_3D\ (g) + DCl\ (g)$ $(-O-)_3AlO\ (s) + 1.5\ D_2O\ (g) \rightarrow\ (-O-)_{1.5}Al(OD)_3\ (s)$	2.44

Appendix B

Reaction mechanism suggestions for $TiCl_4$ – D_2O ALD process

n	**Reactions**	m_0/m_1
0	$TiCl_4$ (g) → $TiCl_4$ (s) $TiCl_4$ (s) + 2 D_2O (g) → –TiO_2 (s) + 4 DCl (g)	0.42
1	–OD (s) + $TiCl_4$ (g) → –O–$TiCl_3$ (s) + DCl (g) –O–$TiCl_3$ (s) + 2 D_2O (g) → (–O–)$_2$Ti(OD) (s) + 3 DCl (g)	0.53
2	2 –OD (s) + $TiCl_4$ (g) → (–O–)$_2$$TiCl_2$ (s) + 2 DCl (g) (–O–)$_2$$TiCl_2$ (s) + 2 D_2O (g) → (–O–)$_2$Ti(OD)$_2$ (s) + 2 DCl (g)	0.72
3	3 –OD (s) + $TiCl_4$ (g) → (–O–)$_3$TiCl (s) + 3 DCl (g) (–O–)$_3$TiCl (s) + 2 D_2O → (–O–)$_2$TiOD (s) + DCl (g)	1.12
4	4 –OD (s) + $TiCl_4$ → (–O–)$_4$$TiO_2$ + 4 DCl (g)	2.51

Appendix C

Reaction mechanism suggestions for $Zr(dmae)_4$ — D_2O ALD process.

n	**Reaction**
0	$Zr(dmae)_4\ (g) \rightarrow Zr(dmae)_4\ (s)$ $Zr(dmae)_4\ (s) + 2\ D_2O\ (g) \rightarrow ZrO_2\ (s) + 4\ dmaeD\ (g)$
1	$–OD\ (s) + Zr(dmae)_4\ (g) \rightarrow –O–Zr(dmae)_3\ (s) + dmaeD\ (g)$ $–O–Zr(dmae)_3\ (s) + 2\ D_2O\ (g) \rightarrow (–O–)_2Zr(OD)\ (s) + 3\ dmaeD\ (g)$
2	$2\ –OD + Zr(dmae)_4\ (g) \rightarrow\ (–O–)_2Zr(dmae)_2\ (s) + 2\ dmaeD\ (g)$ $(–O–)_2Zr(dmae)_2\ (s) + 2\ D_2O\ (g) \rightarrow (–O–)_2Zr(OD)_2\ (s) + 2\ dmaeD\ (g)$
3	$3\ –OD\ (s) + Zr(dmae)_4\ (g) \rightarrow (–O–)_3Zr(dmae)\ (s) + 3\ dmaeD\ (g)$ $(–O–)_3Zr(dmae)\ (s) + 2\ D_2O\ (g) \rightarrow (–O–)_2Zr(OD)_3\ (s) + dmaeD\ (g)$
4	$4\ –OD\ (s) + Zr(dmae)_4\ (g) \rightarrow (–O–)_4Zr–O_2\ (s) + 4\ dmaeD\ (g)$ $(–O–)_4Zr–O_2\ (s) + 2\ D_2O\ (g) \rightarrow (–O–)_2Zr(OD)_4\ (s)$

Appendix D

Reaction mechanism suggestions for $Zr(dmae)_2(O^tBu)_2$ — D_2O ALD process.

n	Reaction
0	$Zr(dmae)_2(O^tBu)_2\ (g) \rightarrow Zr(dmae)_2(O^tBu)_2\ (s)$ $Zr(dmae)_2(O^tBu)_2\ (s) + 2\ D_2O \rightarrow ZrO_2\ (s) + 2\ dmaeD\ (g) + 2\ Bu^tOD\ (g)$
1	$–OD\ (s) + Zr(dmae)_2(O^tBu)_2\ (g) \rightarrow –O–Zr(dmae)_2(O^tBu)\ (s) + Bu^tOD\ (g)$ $–O–Zr(dmae)_2(O^tBu)\ (s) + 2\ D_2O\ (g) \rightarrow (–O–)_2Zr(OD)\ (s) + 2\ dmaeD\ (g) + Bu^tOD\ (g)$
1	$–OD\ (s) + Zr(dmae)_2(O^tBu)_2\ (g) \rightarrow –O–Zr(dmae)(O^tBu)_2\ (s) + dmaeD\ (g)$ $–O–Zr(dmae)(O^tBu)_2\ (s) + 2\ D_2O\ (g) \rightarrow (–O–)_2Zr(OD)\ (s) + dmaeD\ (g) + 2\ Bu^tOD\ (g)$
2	$2\ –OD + Zr(dmae)_2(O^tBu)_2\ (g) \rightarrow\ (–O–)_2Zr(dmae)_2\ (s) + 2\ Bu^tOD\ (g)$ $(–O–)_2Zr(dmae)_2\ (s) + 2\ D_2O\ (g) \rightarrow (–O–)_2Zr(OD)_2\ (s) + 2\ dmaeD\ (g)$
2	$2\ –OD + Zr(dmae)_2(O^tBu)_2\ (g) \rightarrow\ (–O–)_2Zr(O^tBu)_2\ (s) + 2\ dmaeD\ (g)$ $(–O–)_2Zr(O^tBu)_2\ (s) + 2\ D_2O\ (g) \rightarrow (–O–)_2Zr(OD)_2\ (s) + 2\ Bu^tOD\ (g)$
2	$2\ –OD\ (s) + Zr(dmae)_2(O^tBu)_2\ (g) \rightarrow (–O–)_2Zr(dmae)(O^tBu)\ (s) + dmaeD\ (g) + Bu^tOD\ (g)$ $(–O–)_2Zr(dmae)(O^tBu)\ (s) + 2\ D_2O\ (g) \rightarrow (–O–)_2Zr(OD)_2\ (s) + dmaeD\ (g) + Bu^tOD\ (g)$
3	$3\ –OD\ (s) + Zr(dmae)_2(O^tBu)_2\ (g) \rightarrow (–O–)_3Zr(dmae)\ (s) + dmaeD\ (g) + 2\ Bu^tOD\ (g)$ $(–O–)_3Zr(dmae)\ (s) + 2\ D_2O\ (g) \rightarrow (–O–)_2Zr(OD)_3\ (s) + dmaeD\ (g)$
3	$3\ –OD\ (s) + Zr(dmae)_2(O^tBu)_2\ (g) \rightarrow (–O–)_3Zr(dmae)\ (s) + 2\ dmaeD\ (g) + Bu^tOD\ (g)$ $(–O–)_3Zr(O^tBu)\ (s) + 2\ D_2O\ (g) \rightarrow (–O–)_2Zr(OD)_3\ (s) + Bu^tOD\ (g)$
4	$4\ –OD\ (s) + Zr(dmae)_2(O^tBu)_2\ (g) \rightarrow (–O–)_4Zr–O_2\ (s) + 2\ dmaeD\ (g) + 2\ Bu^tOD\ (g)$ $(–O–)_4Zr–O_2\ (s) + 2\ D_2O\ (g) \rightarrow (–O–)_2Zr(OD)_4\ (s)$

Appendix E

Reaction mechanism suggestions for $Zr(dmae)_2(O^iPr)_2$ — D_2O ALD process.

n	**Reaction**
0	$Zr(dmae)_2(O^iPr)_2\ (g) \rightarrow Zr(dmae)_2(O^iPr)_2\ (s)$ $Zr(dmae)_2(O^iPr)_2\ (s) \rightarrow ZrO_2\ (s) + 2\ Pr^iOD\ (g) + 2\ dmaeD\ (g)$
1	$–OD\ (s) + Zr(dmae)_2(O^iPr)_2\ (g) \rightarrow –O–Zr(dmae)_2(O^iPr)\ (s) + Pr^iOD$ $–O–Zr(dmae)_2(O^iPr)\ (s) + 2\ D_2O\ (g) \rightarrow (–O–)_2Zr(OD)\ (s) + 2\ dmaeD\ (g) + Pr^iOD\ (g)$
1	$–OD\ (s) + Zr(dmae)_2(O^iPr)_2\ (g) \rightarrow –O–Zr(dmae)(O^iPr)_2\ (s) + dmaeD\ (g)$ $–O–Zr(dmae)(O^iPr)_2\ (s) + 2\ D_2O\ (g) \rightarrow (–O–)_2Zr(OD)\ (s) + dmaeD\ (g) + 2\ Pr^iOD\ (g)$
2	$2\ –OD + Zr(dmae)_2(O^iPr)_2\ (g) \rightarrow\ (–O–)_2Zr(dmae)_2\ (s) + 2\ Pr^iOD\ (g)$ $(–O–)_2Zr(dmae)_2\ (s) + 2\ D_2O\ (g) \rightarrow (–O–)_2Zr(OD)_2\ (s) + 2\ dmaeD\ (g)$
2	$2\ –OD + Zr(dmae)_2(O^iPr)_2\ (g) \rightarrow (–O–)_2Zr(O^iPr)_2\ (s) + 2\ dmaeD\ (g)$ $(–O–)_2Zr(O^iPr)_2\ (s) + 2\ D_2O\ (g) \rightarrow (–O–)_2Zr(OD)_2\ (s) + 2\ Pr^iOD\ (g)$
2	$2\ –OD\ (s) + Zr(dmae)_2(O^iPr)_2\ (g) \rightarrow (–O–)_2Zr(dmae)(O^iPr)\ (s) + dmaeD\ (g) + Pr^iOD\ (g)$ $–O_2–Zr(dmae)(O^iPr)\ (s) + 2\ D_2O\ (g) \rightarrow –O_2–Zr(OD)_2\ (s) + dmaeD\ (g) + DO^iPr\ (g)$
3	$3\ –OD\ (s) + Zr(dmae)_2(O^iPr)_2\ (g) \rightarrow (–O–)_3Zr(dmae)\ (s) + dmaeD\ (g) + 2\ Pr^iOD\ (g)$ $(–O–)_3Zr(dmae)\ (s) + 2\ D_2O\ (g) \rightarrow (–O–)_2Zr(OD)_3\ (s) + dmaeD\ (g)$
3	$3\ –OD\ (s) + Zr(dmae)_2(O^iPr)_2\ (g) \rightarrow (–O–)_3Zr(O^iPr)\ (s) + 2\ dmaeD\ (g) + Pr^iOD\ (g)$ $(–O–)_3Zr(O^iPr)\ (s) + 2\ D_2O\ (g) \rightarrow (–O–)_2Zr(OD)_3\ (s) + Pr^iOD\ (g)$
4	$4\ –OD\ (s) + Zr(dmae)_2(O^iPr)_2\ (g) \rightarrow (–O–)_4Zr–O_2\ (s) + 2\ dmaeD\ (g) + 2\ Pr^iOD\ (g)$ $(–O–)_4Zr–O_2\ (s) + 2\ D_2O\ (g) \rightarrow (–O–)_2Zr(OD)_4\ (s)$